Quantitative Finance

ISSN: 1469-7688 (Print) 1469-7696 (Online) Journal homepage: https://www.tandfonline.com/loi/rquf20

Detecting intraday financial market states using temporal clustering

D. Hendricks, T. Gebbie & D. Wilcox

Quantitative Finance, 2016
Vol. 16, No. 11, 1657–1678, http://dx.doi.org/10.1080/14697688.2016.1171378

Detecting intraday financial market states using temporal clustering

D. HENDRICKS*, T. GEBBIE and D. WILCOX

School of Computer Science and Applied Mathematics, University of the Witwatersrand, Johannesburg WITS 2050, South Africa

(*Received 19 August 2015; accepted 17 March 2016; published online 27 April 2016*)

We propose the application of a high-speed maximum likelihood clustering algorithm to detect temporal financial market states, using correlation matrices estimated from intraday market microstructure features. We first determine the *ex-ante* intraday temporal cluster configurations to identify market states, and then study the identified temporal state features to extract *state signature vectors* (SSVs) which enable online state detection. The *SSVs* serve as low-dimensional state descriptors which can be used in learning algorithms for optimal planning in the high-frequency trading domain. We present a feasible scheme for real-time intraday state detection from streaming market data feeds. This study identifies an interesting hierarchy of system behaviour which motivates the need for timescale-specific state space reduction for participating agents.

Keywords: Market microstructure; Temporal clustering; Financial market states; State space reduction

JEL Classification: C61, C63, D81, G10

1. Introduction

The financial market represents a prime example of an observable complex adaptive system. Many heterogeneous adaptive agents, such as traders, portfolio managers, market makers and regulatory authorities, interact non-linearly over time with each other and the electronic exchange allowing for the emergence of complex behaviours beyond that expected based on intrinsic agent characteristics. Many authors have viewed financial markets through this lens, considering analogues with physical systems to formulate models which aid our understanding of observed system characteristics (see Arthur (1995), Arthur *et al*. (1997), Brock (1993), Hommes (2001), Wilcox and Gebbie (2014) and the references therein). Recent technological advances, accelerated by a highly competitive industry, have allowed for the efficient generation, storage and retrieval of financial data at micro timescales, providing a rich record of the price formation process as a laboratory for intensive study. The field of market microstructure developed to study the characteristics and behaviours of financial system dynamics at this scale (see O'Hara (1998), Madhavan (2000), Biais *et al*. (2005), Hinton (2007), Gençay *et al*. (2010), Baldovin *et al*. (2015) for a comprehensive discussion). In particular, as intraday trading and investment processes become increasingly automated, understanding the system dynamics at varying intraday timescales is critical for an efficient trajectory through the system to be mapped by participating agents.

This paper aims to use a physical analogy to the ferromagnetic Potts model at thermal equilibrium to describe object interactions, before deriving an unsupervised clustering algorithm, where both the number of clusters and configuration emerges from the data (Blatt *et al*. 1996, 1997, Wiseman *et al*. 1998, Giada and Marsili 2001). Treating intraday time periods as objects, the algorithm will be used to identify intraday market states from observed market microstructure features. Although Marsili (2002) used a similar approach to classify days as states, the authors are unaware of another study which applies this technique to *intraday* period clustering using *multiple* features. In addition, a high-speed parallel genetic algorithm (PGA) will be used for efficient computation of the cluster configurations, with absolute computation speeds conducive to overnight or even intraday recalibration of identified states (Hendricks *et al*. 2016).

The results reveal an interesting hierarchy of system behaviour at different timescales. Statistically significant power-law fits to configuration characteristics suggest scale-invariant behaviour which may translate to persistent features in market states. In addition, the power-law fits yield different scaling exponents at the different timescales, suggesting that the system may be at criticality at each scale, possibly with different universality classes characterizing behaviour (Dacorogna *et al*. 1996, Gabaix *et al*. 2003, Emmert-Streib and Dehmer 2010,

*Corresponding author. Email: dieter.hendricks@students.wits.ac.za

Mastromatteo and Marsili 2011). This motivates the importance of timescale-specific information when planning in this domain. Here we are considering a particular case of *calendar time* when investigating scale-related phenomena; however, we note that there are alternative scales used to measure the financial system. There is a rich history in the literature which has aimed to directly model the *event time* foundations of market microstructure processes. The seminal work of Garman (1976), which used point processes to model order book events, forms the basis of many subsequent *event time* approaches to modelling transaction and quote data. An important extension of this view is the vector autoregressive model for trades and quotes developed by Hasbrouck (1988, 1991) and Engle and Russell (1998). A complementary approach introduces the concept of *intrinsic time*, which aims to measure trading opportunities in reference to specific features of traded stocks, for example, using the rate of trading to modify calendar or chronological time. These are discussed by Müller *et al*. (1995) and Derman (2002). The more recent use of Hawkes processes to model mutually-exciting order book events is an important return to the idea of viewing events as a foundational concept when modelling transactions and order book dynamics (Large 2000, Toke and Pomponio 2012, Abergel and Jedidi 2015, Bacry *et al*. 2015).

Easley *et al*. (2012) introduce the *volume time* paradigm for high-frequency trading, with the clock ticking according to the number of events (proxied by trade volume) flowing through the system. This is a pragmatic attempt to reconcile the foundational event-based paradigm introduced by Garman (1976) with the wide use of chronological or calendar time. They argue that machines operate on a clock which is not chronological, but rather related to the number of cycles per instruction initiated by an event (Easley *et al*. 2012, Patterson and Hennessy 2013). This allows one to measure time in terms of frequency of changes in information, as measured by trading volumes. When one considers the *complex event processing* paradigm which underpins many automated trading systems in financial markets (Adi *et al*. 2006), one can appreciate the suitability of the event-based clock and the view that the calendar time clock is a legacy convenience from the low-frequency, human-trader-driven world. As the shift from human-driven to machine-driven trading dominates financial markets, the study of event-timescale phenomena has become increasingly important and warrants further exploration.

While the identified market states reveal many interesting insights, trading agents would benefit from being able to detect online (or in real-time) which state they are *currently* in. We develop a novel technique which extracts the characteristic signature of market activity from each of the identified states, and uses this as the basis for an online state detection algorithm. In one application, this is used to construct 1-step transition probability matrices, which can be refined online and used in optimal planning algorithms.

This paper proceeds as follows: section 2 describes a non-parametric clustering approach using a physical Potts model analogy. Section 3 uses the Potts model analogy to derive a maximum likelihood estimator for the optimal cluster configuration. Section 4 describes the idea of clustering time periods as objects in order to identify market states. Section 5 describes the parallel genetic algorithm (PGA) for high-speed detection of the temporal cluster configuration using the maximum likelihood estimator. Section 6 describes an approach for online state detection. Section 7 discusses scale-invariant properties of the cluster configurations and how these may be exploited for efficient online state detection. Section 8 discusses the data used, workflow and results. Section 9 provides some concluding remarks and suggestions for further research.

2. Super-paramagnetic clustering

Blatt *et al*. (1996, 1997) and Wiseman *et al*. (1998) proposed a novel non-parametric clustering approach, based on an analogy to the ferromagnetic Potts model at thermal equilibrium. By assigning a Potts spin variable to each object and introducing a short-range distance-dependent ferromagnetic interaction field, regions of aligned spins emerge, which are analogous to groups of objects in the same cluster, where *spin alignment* suggests *object homogeneity* (Wang and Swendsen 1990).

More formally, consider a q-state Potts model with spins $s_i = 1, \dots, q$ for $i = 1, \dots, N$, where N is the total number of objects in the system. The cost function is given by the following Hamiltonian:

$$H = - \sum_{s_i, s_j \in S} J_{ij} \delta(s_i, s_j) \qquad (1)$$

where the spins s_i can take on q-states and the coupling of the ith and jth object is governed by J_{ij}. In the case of object clustering for a data sample, a candidate configuration is given by the set $\mathcal{S} = \{s_i\}_{i=1}^{n}$, where s_i represents the cluster group index to which the ith object belongs. One can consider the coupling parameters J_{ij} as being a function of the correlation coefficient C_{ij} (Kullmann *et al*. 2000, Giada and Marsili 2001). This is used to specify a distance function that is decreasing with distance between objects. If all the spins are related in this way, then each pair of spins is connected by some non-vanishing coupling $J_{ij} = J_{ij}(C_{ij})$. This allows one to interpret s_i as a Potts spin in the Potts model Hamiltonian with J_{ij} decreasing with the distance between objects (Blatt *et al*. 1996, Kullmann *et al*. 2000). The case where there is only one cluster can be thought of as a ground state. As the system becomes more excited, it could break up into additional clusters. Each cluster would have specific Potts magnetizations, even though the net magnetization can be zero for the complete system. Generically, the correlation would then be both a function of time and temperature in order to encode both the evolution of clusters, as well as the hierarchy of clusters as a function of temperature. In the basic approach, one is looking for the lowest energy state that fits the data.

3. A maximum likelihood approach

In order to parameterize the model efficiently, one can choose to make an ansatz for the data generative function (Noh 2000) and use this to develop a maximum-likelihood approach (Giada and Marsili 2001), rather than explicitly solving the Potts Hamiltonian numerically (Blatt *et al*. 1996, Kullmann *et al*. 2000). A number of authors have considered this approach for object clustering (McLachlan *et al*. 1996, Giada and Marsili 2001, Mungan and Ramasco 2010), however we follow the proposition by Giada and Marsili (2001). A summary exposition will be presented here (as shown in Hendricks *et al*. (2016)), with a full derivation available in the appendices.

According to the Noh (2000) ansatz, the generative model of the time series associated with the ith object can then be written as

$$x_i(t) = g_{s_i}\eta_{s_i} + \sqrt{1 - g_{s_i}^2}\epsilon_i \tag{2}$$

where the cluster-related influences are driven by η_{s_i} and the object-specific effects by ϵ_i, both treated as Gaussian random variables with unit variance and zero mean.† The relative contribution is controlled by the intra-cluster coupling parameter g_{s_i}. The Noh–Giada–Marsili model encodes the idea that objects which have something in common belong in the same cluster, object membership in a particular cluster is mutually exclusive and intra-cluster correlations are positive.

If one takes equation (2) as a statistical hypothesis, it is possible to compute the probability density $P(\{\bar{x}_i\}|\mathcal{G},\mathcal{S})$ for any given set of parameters $(\mathcal{G},\mathcal{S}) = (\{g_s\},\{s_i\})$ by observing the data-set $\{x_i\}$, $i, s = 1,\ldots,N$ as a realization of the common component of equation (2) as follows (Giada and Marsili 2001):

$$P(\{\bar{x}_i\}|\mathcal{G},\mathcal{S}) = \prod_{d=1}^{D}\left\langle \prod_{i=1}^{N}\delta\left(x_i(t) - g_{s_i}\bar{\eta}_{s_i} + \sqrt{1-g_{s_i}^2}\bar{\epsilon}_i\right)\right\rangle. \tag{5}$$

In equation (5), N is the number of objects and D is the number of feature measurements for each object. The variable δ is the Dirac delta function and $\langle\ldots\rangle$ denotes the mathematical expectation. For a given cluster structure $\mathcal{S}$, the likelihood is maximal when the parameter g_s takes the values

$$g_s^* = \begin{cases}\sqrt{\frac{c_s-n_s}{n_s^2-n_s}} & \text{for } n_s > 1,\\ 0 & \text{for } n_s \leq 1.\end{cases} \tag{6}$$

n_s in equation (6) denotes the number of objects in cluster s, i.e.

$$n_s = \sum_{i=1}^{N}\delta_{s_i,s}. \tag{7}$$

The variable c_s is the internal correlation of the sth cluster, denoted by the following equation:

$$c_s = \sum_{i=1}^{N}\sum_{j=1}^{N}C_{ij}\delta_{s_i,s}\delta_{s_j,s}. \tag{8}$$

†This form of the price model ensures that the self-correlation of a stock is one and independent of the cluster coupling. This can be seen by computing the self correlation $E[x_i^2]$ and using that clusters and stock unique process are unit variance zero mean processes

$$\mathrm{E}\left[\left(g_{s_i}\eta_{s_i} + \sqrt{1-g_{s_i}^2}\epsilon_i\right)^2\right] = g_{s_i}^2 + (1-g_{s_i}^2) = 1. \tag{3}$$

This is not a unique choice, another possible choice often used is

$$\mathrm{E}\left[\left(\frac{\sqrt{g_{s_i}}}{\sqrt{1+g_{s_i}}}\eta_{s_i} + \frac{1}{\sqrt{1+g_{s_i}}}\epsilon_i\right)^2\right] = \frac{1+g_{s_i}}{1+g_{s_i}} = 1. \tag{4}$$

The variable C_{ij} is the *Pearson correlation coefficient* of the data, denoted by the following equation:

$$C_{ij} = \frac{\bar{x_i}\bar{x_j}}{\sqrt{\|\bar{x_i}^2\|\|\bar{x_j}^2\|}}. \tag{9}$$

The maximum likelihood of structure $\mathcal{S}$ can be written as $P(\mathcal{G}^*,\mathcal{S}|\bar{x_i}) \propto \exp^{D\mathcal{L}(\mathcal{S})}$, where the resulting likelihood function per feature $\mathcal{L}_c$ is denoted by

$$\mathcal{L}_c(\mathcal{S}) = \frac{1}{2}\sum_{s:n_s>1}\left(\log\frac{n_s}{c_s} + (n_s-1)\log\frac{n_s^2-n_s}{n_s^2-c_s}\right). \tag{10}$$

From equation (10), it follows that $\mathcal{L}_c = 0$ for clusters of objects that are uncorrelated, i.e. where $g_s^* = 0$ or $c_s = n_s$ or when the objects are grouped in singleton clusters for all the cluster indexes ($n_s = 1$). Equations (8) and (10) illustrate that the resulting maximum likelihood function for $\mathcal{S}$ depends on the *Pearson correlation coefficient* C_{ij} and hence exhibits the following advantages in comparison to conventional clustering methods:

- It is **unsupervised**: The optimal number of clusters is unknown *a priori* and not fixed at the outset
- The interpretation of results is **transparent** in terms of the model, namely equation (2).

Giada and Marsili state that $\max_s \mathcal{L}_c(\mathcal{S})$ provides a measure of structure inherent in the cluster configuration represented by the set $\mathcal{S} = \{s_1,\ldots,s_n\}$ (Giada and Marsili 2001). The higher the value, the more pronounced the structure.

We note that the particular choice of Gaussian innovations in equation (2) is convenient, since the *Pearson correlation coefficient* then completely characterizes pairwise interactions amongst objects in the system (Giada and Marsili 2001). This is a necessary condition, given the physical analogy and link to the motivating Hamiltonian given in equation (1). The application of this technique to high-frequency financial time series may motivate a more prudent assumption for the underlying object and cluster dynamics, incorporating jumps to better model the price formation process at this scale. However, the use of, say, jump diffusion innovations would require an alternative dependency metric, such as Lévy copulas, to completely capture object interactions (Cont and Tankov 2004, McNeil *et al*. 2015), requiring a careful rederivation of the appropriate likelihood function. This will be explored in further research.

4. Detecting temporal states using clustering

The data generative model specified by equation (2) is sufficiently generic that it can be applied to a diverse set of problem domains, where object and cluster innovations can be assumed to be Gaussian. In the financial domain, initial applications focused on clustering stocks based on price changes (Giada and Marsili 2001, Hendricks *et al*. 2016), however Marsili (2002) proposed that this technique could be used to cluster *time periods* in order to identify *temporal market states*. Days were grouped into clusters based on the closing price performance of the chosen universe of stocks, demonstrating a meaningful classification of market-wide activity which persists through time (Marsili 2002). We propose that a similar approach can be applied to discover *intraday* temporal states, clustering time periods based on the performance of *multiple* observable market microstructure features. A practical trading system often has access to a real-time market data feed, from which multiple features can be extracted to describe various aspects of the evolving limit order book. In addition, examining temporal cluster configurations at varying timescales can suggest a hierarchy of system behaviour, providing insights into exogenous and endogenous market activity. This can also assist trading agents in developing optimal trajectories for varying objectives, such as stock acquisition or liquidation at minimal cost. In particular, for an agent tasked to learn an optimal policy (state-action mapping), the grouping of temporal periods into market states based on market microstructure feature performance provides a novel scheme to reduce the dimensionality of the state space and promote efficient learning.

In this paper, we will focus on the emergent hierarchy of system behaviour at different timescales and explore a scheme for online state detection. In one application, this leads to a system of 1-step state transition probability matrices at varying scales, which can be refined online in real-time. These can be used in optimal planning schemes where Markovian dynamics are assumed and state persistence can be exploited.

5. A high-speed PGA implementation

The likelihood function specified in equation (10) serves as the objective function in a metaheuristic optimization routine, where candidate cluster configurations are evaluated and successively improved until a configuration best explains the inherent structure in a given correlation matrix. Giada and Marsili (2001) used simulated annealing and deterministic maximization to approximate the maximum likelihood structure. While appropriate for their study, these techniques are inherently computationally intensive and may require a significant amount of time to converge for large-scale problems. In addition, it is unclear whether such trajectory-based methods are appropriate for the multi-featured clustering problem considered in this paper, since Giada and Marsili (2001) clustered objects (stocks) based on a single feature (price returns). Hendricks *et al*. (2016) and Cieslakiewicz (2014) propose the use of a high-speed PGA, leveraging the streaming multiprocessors (SMs) of a graphics processing unit (GPU), where equation (10) is used as a fitness function to find the cluster configuration which best approximates the maximum likelihood structure. They implemented a C-based master-slave PGA using the Nvidia compute unified device architecture (CUDA) development environment, using the single program multiple data (SPMD) architecture to enumerate the GPU thread hierarchy with population members for concurrent application of genetic operators.

Consider the problem of finding the cluster configuration of n objects. Then, given N candidate cluster configuration structures making up the population,

$$\begin{aligned}
\mathcal{S}_1 &= \{s_1^1, \ldots, s_n^1\} \\
\mathcal{S}_2 &= \{s_1^2, \ldots, s_n^2\} \\
&\vdots \\
\mathcal{S}_N &= \{s_1^N, \ldots, s_n^N\}
\end{aligned}$$

would be mapped to the GPU thread hierarchy using a two-dimensional grid, as shown in table 1.

The PGA was applied to the relatively small problem of finding the cluster configuration of 18 objects, however demonstrated fast absolute computation time compared to state-of-the-art methods, with the promise of scalability within the constraints of the GPU architecture used (Cieslakiewicz 2014, Hendricks *et al*. 2016). We have restricted our analysis to intraday temporal periods within one month, however this still yields up to 2208 objects in the 5-min case. Table 2 shows the specifications and capabilities of the two candidate GPUs and table 3 shows the PGA parameter values and number of objects for each of the timescales investigated. The mapping of candidate configurations to the GPU thread hierarchy under the SPMD paradigm results in an upper bound on the permissible number of objects and population size. Hendricks *et al*. (2016) further recognized the importance of ensuring that the population size is large enough relative to the number of objects, to ensure sufficient population diversity for convergence to the best approximation of the maximum likelihood structure within a finite number of generations. Smaller populations often lead to suboptimal algorithm terminations and inconsistent results. For the 60-min, 30-min and 15-min cases, the Nvidia Geforce GTX765m notebook GPU had sufficient capability to determine the optimal cluster configurations from sufficiently large populations. The 5-min case demanded a larger capacity GPU, and the Nvidia Geforce GTX Titan X provided the necessary additional SMs, CUDA cores and global memory to facilitate efficient computation.

We note that the number of generations and stall generations indicated in table 3 is higher than one would typically specify for a genetic algorithm, since these promote potential over-fitting to the prescribed dataset. Recall that our application is to find the candidate cluster configuration which best explains the structure inherent in a given correlation matrix. Thus we

Table 1. Mapping of population to CUDA thread hierarchy.

	CUDA thread block grid			
	$\mathcal{S}_1$	$\mathcal{S}_2$	…	$\mathcal{S}_N$
$object_1$	s_1^1	s_1^2	…	s_1^N
$object_2$	s_2^1	s_2^2	…	s_2^N
$\vdots$	$\vdots$	$\vdots$	…	$\vdots$
$object_n$	s_n^1	s_n^2	…	s_n^N

Table 2. GPU specification and capabilities.

Feature	GPU	
	Nvidia Geforce GTX 765m	Nvidia Geforce GTX Titan X
Compute capability	3.5	5.2
CUDA cores	768	3072
Memory	2048MB	12 228MB
Number of SMs	16	96
Max threads/thread block	1024	1024
Thread block dimension	32	32
Max thread blocks/multiprocessor	16	32

Table 3. Parameter values and computation times for PGA.

Time scale	Number of periods (objects)	Population size	Generations	Stall generations	Mutation probability	Crossover probability	Computation Time (s)∗
5-min	2208	4000	4000	1000	0.09	0.9	603 (*D*)
15-min	736	1000	4000	500	0.09	0.9	382 (*N*)
30-min	368	800	4000	500	0.09	0.9	215 (*N*)
60-min	184	600	4000	500	0.09	0.9	132 (*N*)

∗ Average from 20 independent runs; *N* refers to the GTX765m Notebook GPU and *D* refers to the GTX Titan X Desktop GPU.

Figure 1. Illustration of online state assignment based on identified SSVs.

are not concerned with out-of-sample validity, but would rather prefer to find a configuration with the highest likelihood value. The higher number of generations and stall generations, together with the mutation operator, promotes convergence to a higher likelihood structure. The average computation times indicated in table 3 are not overly onerous, suggesting that for practical application, overnight or even intraday estimation of cluster configurations to capture recent dynamics is feasible. The proposed PGA thus offers an efficient, scalable alternative for finding the best approximation of the optimal cluster configuration, suitable for clustering objects on multiple observable features.

6. State signature vectors (SSVs) for online state detection

The clustering procedure described thus far can be used as an unsupervised algorithm to group temporal periods into states according to feature similarity; however, this can only reveal the *ex-ante* temporal states and is not suitable for online detection. Upon examination of the resulting cluster configurations, we noted that each node refers to a particular time period, with an associated signature of market activity. Furthermore, if two time periods appear in the same cluster, given the data generative model assumed in equation (2), we conjecture that it is the relative similarity of their characteristic signatures of market activity which resulted in their assignment to the same cluster. Using this idea, given a cluster configuration of temporal periods into market states, it is possible to extract a *SSV* which summarizes the signature of market activity across stocks and time periods for each state. Then, if one is faced with a new candidate feature vector (FV), the market state assignment can be determined by using the closest match within the set of pre-determined SSVs computed offline. FVs are easy to compute online from a streaming datafeed and state assignment can be achieved using a simple Euclidean distance computation. To make these ideas concrete, consider the example illustrated in figure 1.

Here, we compute two SSVs from the identified states, and use these as a basis for assigning a new FV to a market state. This is based on a simple Euclidean distance metric,

$$\text{argmin}_p ||FV - SSV_p||,$$

where p is the index of the identified states.

In this paper, we have used four features to characterize market activity at intraday scale. These include: *trade price, trade volume, spread* and *quote volume imbalance*. In particular, we consider the *relative change* in each of these features. For example, based on a set of feature measurements $\mathcal{F}^{5\,\text{min}}$ at 5-min scale, we would compute

$$\triangle f_t^{5\,\text{min}} = \frac{f_t^{5\,\text{min}} - f_{t-1}^{5\,\text{min}}}{f_{t-1}^{5\,\text{min}}}$$

for all $f_t^{5\,\text{min}} \in \mathcal{F}^{5\,\text{min}}$. For the initial temporal cluster detection stage, these "feature returns" are calculated for each stock and concatenated before computing the time period correlation matrix.

For the extraction of SSVs from significant states, we compute average feature returns across member periods and stocks. For example, consider the case of 15-min period clustering. If one state (cluster) consisted of 2 periods (09:15–09:30 and 15:15–15:30), then we would find the average *trade price, trade volume, spread* and *quote volume imbalance* returns across stocks in each period (i.e. two 4-element vectors), then average across these two vectors to get a single four-element vector, which would be the representative SSV for that state.

Although this results in a loss of information, we conjecture that the average signature of feature returns broadly captures the state of market activity. The SSVs for each timescale configuration are illustrated in figures 3, 5, 7 and 9. Following this approach, the FVs calculated in the online environment would constitute the same averages of feature returns, before matching to the appropriate SSV. We note that this is merely one candidate scheme for extracting SSVs which are conducive to online matching for state assignment; however, alternative schemes for extraction of SSVs which preserve state-specific information will be explored in future work. The chosen features do not represent an exhaustive set of possible explanatory factors for intraday market activity, but rather were chosen based on the relative ease of their online construction from streaming Level-1 market data feeds JSE (2015). Additional features can be considered in future work.

7. Scale-invariant characteristics of states

The detected temporal cluster configurations can be further analysed to determine whether any characteristics exhibit scale-invariant behaviour. In particular, a visual inspection of the cluster configurations shown in section 8.3 led us to conjecture a possible power-law fit for cluster sizes. Many physical and man-made systems exhibit characteristics which follow a power-law functional form, and its unique mathematical properties sometimes lead to surprising physical insights (Gabaix *et al*. 2003, Clauset *et al*. 2009). Many authors have investigated the nature of information and forecasting at different time scales in financial markets (see Dacorogna *et al.* (1996), Zhang *et al*. (2005), Emmert-Streib and Dehmer (2010) as examples). For our application, the existence of different critical exponents for the best power-law fits at different timescales may suggest different universality classes which characterize the system activity at each scale. In fact, Mastromatteo and Marsili (2011) discuss the notion that, for a complex adaptive system, distinguishable models can only be gleaned when the system is near criticality. Thus, if financial markets truly are a complex adaptive system, measurable quantities from the dynamics at each scale should yield a statistically significant power-law fit. Although it is difficult to quantify the exact nature of these scale-specific behaviours or universality classes, their apparent existence suggests that investment and trading decisions would benefit from timescale-specific state space information. This would enhance the efficacy of intraday policies which aim to find optimal trajectories through the system.

Given the difficulties of identifying statistically significant power-law fits to empirical quantities (Bauke 2007), we incorporated the maximum likelihood fitting procedure provided by Clauset *et al*. (2009). Outputs from their functions include the scaling parameter of the proposed power-law fit, a Kolmogorov–Smirnov test for the goodness-of-fit of the proposed model to the data, the lower bound for the fit if the tail distribution follows a power-law and the log-likelihood of the data under the power-law fit.

We note that a detected temporal cluster configuration results in a set of homogeneous market states, although it is not clear which states are significant, i.e. likely to persist, or merely transient. Using *all* identified states may result in spurious state assignments if one uses the online algorithm described in section 6. This leads to the need for some selection criteria for significant states, before extracting SSVs. Candidate criteria include using intra-cluster connectedness (c_s) or cluster size with some form of thresholding procedure, however these heuristics are inherently subjective. The power-law fit to cluster size provides one candidate objective approach for state selection. Under the assumption that the system is near criticality when we find a stable parameter calibration, choosing the states which best fit the power-law functional form may aid in isolating those states which best capture the system behaviour at that scale, i.e. filter the stable, persistent states from the noise. This provides an objective mechanism for selecting significant states, reducing the set of SSVs which form the basis for the online state detection algorithm.

8. Data and results

8.1. Data description

The data for this study constituted tick-level trades and top-of-book quotes for 42 stocks on the Johannesburg Stock Exchange (JSE) from 1 November 2012 to 30 November 2012. This data were sourced from the Thomson Reuters Tick History (TRTH) database. The raw data were aggregated according to the timescale considered (5-min, 15-min, 30-min and 60-min), before calculating the required features (change in trade price, trade volume, spread and volume imbalance). The 42 stocks considered represent the prevailing constituents of the FTSE/JSE Top40 headline index, which contains the 42 largest stocks by market capitalization in the main board's FTSE/JSE All-Share index.

The objects of interest for the cluster analysis are the *time periods*. Table 4 provides an example of the required data returns matrix, from which a correlation matrix is computed for time period similarity. This is the only required input for the clustering algorithm.

8.2. Visualization

For the cluster configuration visualization, we made use of the Gephi graph visualization and manipulation software package (Bastian *et al*. 2009), with a customized enumeration of nodes and edges and the Fruchterman and Reingold (1991) node spacing algorithm. The presence of an edge between nodes indicates membership to the same cluster, while edge thickness provides a visual impression of object–object correlation, and hence intra-cluster connectedness. For the visualizations which

Table 4. Illustration of data returns matrix as an input for estimation of 15-min period correlations.

	Feature	Times					
		01-Nov-2012 09:00	01-Nov-2012 09:15	01-Nov-2012 09:30	...	30-Nov-2012 16:30	30-Nov-2012 16:45
Trade Price	AGL trade price return	0.35	0.60	0.85	...	0.39	0.22
	AMS trade price return	0.94	0.71	0.73	...	0.63	0.78
	SBK trade price return	0.70	0.38	0.58	...	0.38	0.81
	⋮	⋮	⋮	⋮	⋮	⋮	⋮
	WHL trade price return	0.90	0.49	0.05	...	0.65	0.53
Spread	AGL spread return	0.64	0.49	0.68	...	0.05	0.95
	AMS spread return	0.33	0.09	0.76	...	0.44	0.97
	SBK spread return	0.09	0.73	0.54	...	0.80	0.48
	⋮	⋮	⋮	⋮	⋮	⋮	⋮
	WHL spread return	0.41	0.61	0.11	...	0.40	0.69
Trade Volume	AGL trade volume return	0.61	0.59	0.96	...	0.65	0.50
	AMS trade volume return	0.16	0.09	0.47	...	0.86	0.57
	SBK trade volume return	0.98	0.05	0.67	...	0.72	0.12
	⋮	⋮	⋮	⋮	⋮	⋮	⋮
	WHL trade volume return	0.38	0.49	0.36	...	0.27	0.81
Volume Imbalance	AGL volume imb return	0.01	0.45	0.78	...	0.69	0.77
	AMS volume imb return	0.54	0.17	0.87	...	0.47	0.44
	SBK volume imb return	0.20	0.42	0.91	...	0.88	0.58
	⋮	⋮	⋮	⋮	⋮	⋮	⋮
	WHL volume imb return	0.20	0.09	0.38	...	0.90	0.12

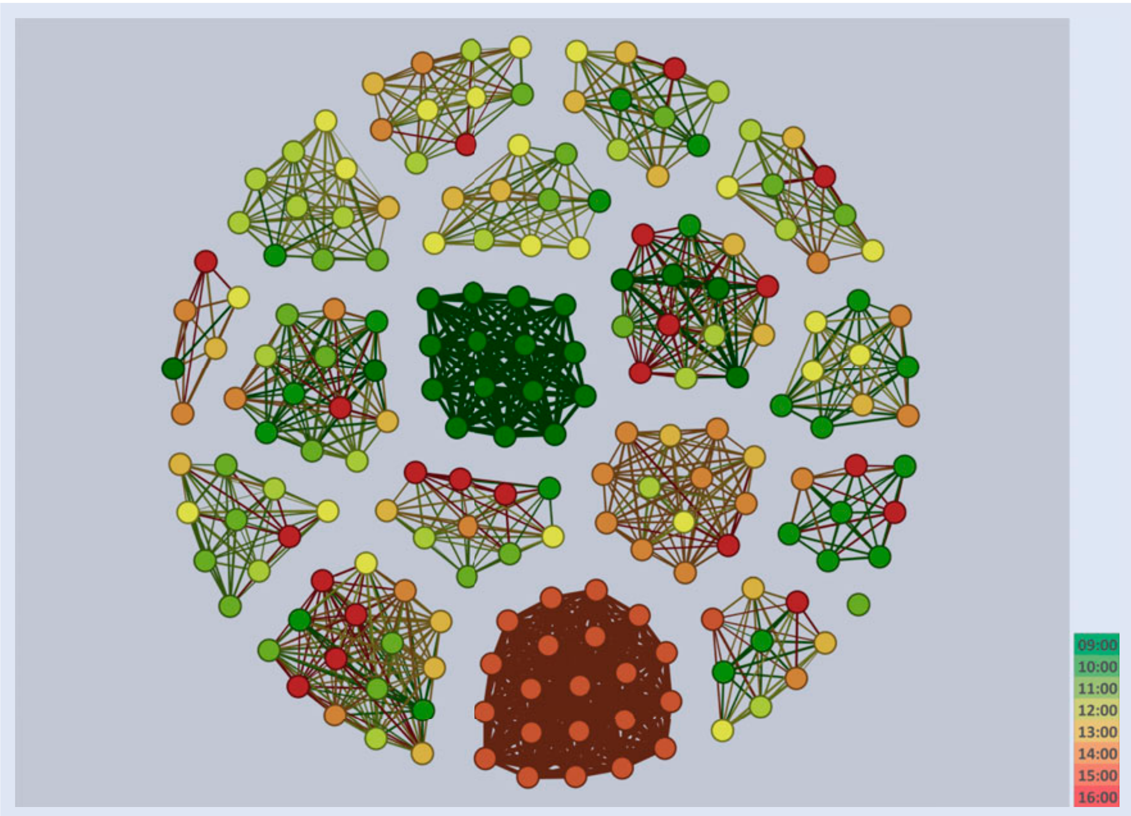

Figure 2. JSE TOP40 60-min temporal clusters for the period 1 November 2012 to 30 November 2012, representing 184 distinct periods. Each node represents a 60-min period during a trading day, with the colour shading indicating the time-of-day (Morning = green, Lunch = yellow, Afternoon = red) and node connectedness indicating cluster membership.

follow, we chose to colour the nodes by intraday time period, in order to illuminate any calendar time effects in the detected states. According to this scheme, the same time on different days will receive the same colour. These visualizations are shown in figures 2, 4, 6, 8, 11–14.

8.3. Results discussion

For each set of results, we consider 8 h of continuous trading activity each day, from 09:00 to 17:00, for the duration of one month. Figure 2 shows the temporal cluster configuration of 60-min periods. We first note that the detection of non-trivial

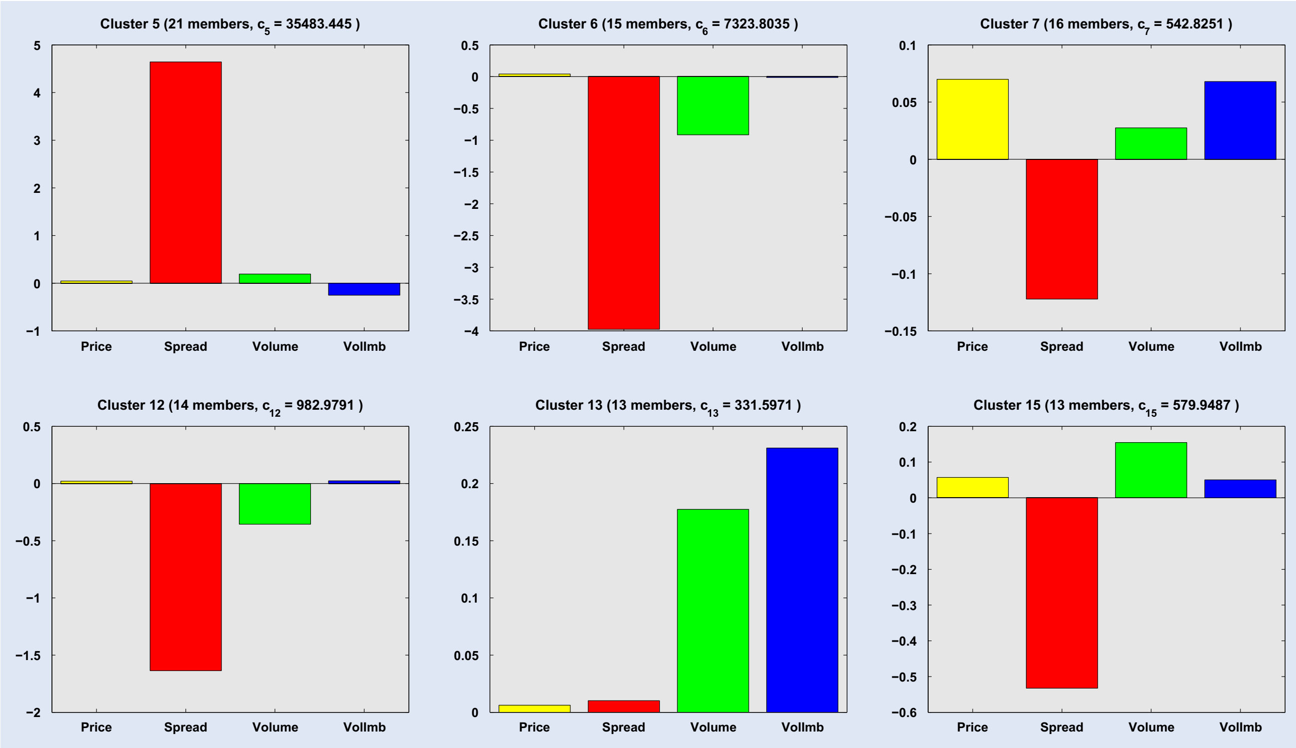

Figure 3. JSE TOP40 60-min cluster SSVs for the period 1 November 2012 to 30 November 2012. Each plot illustrates the average change in trade price, spread, trade volume and quote volume imbalance across member periods and stocks for each of the clusters with a size $\geq x_{\min}$ from the truncated power-law fit. Cluster size and intra-cluster correlation are shown in parentheses.

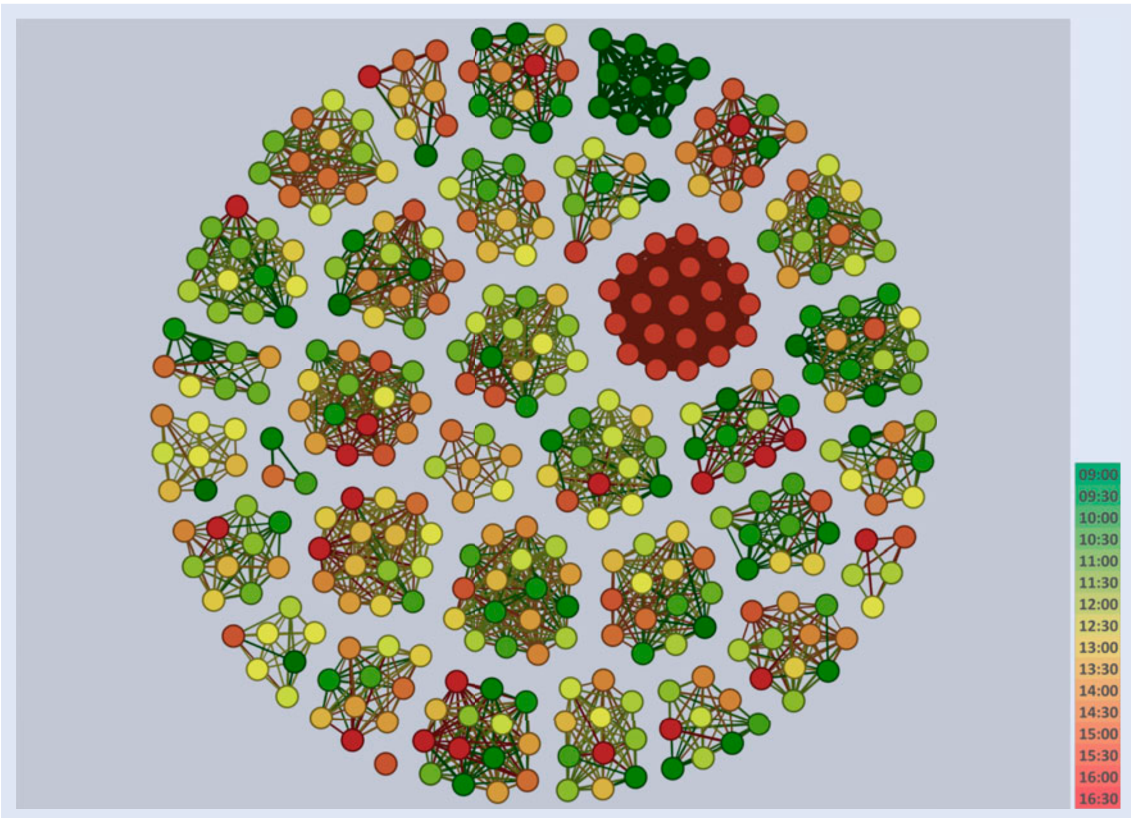

Figure 4. JSE TOP40 30-min temporal clusters for the period 1 November 2012 to 30 November 2012, representing 368 distinct periods. Each node represents a 30-min period during a trading day, with the colour shading indicating the time-of-day (Morning = green, Lunch = yellow, Afternoon = red) and node connectedness indicating cluster membership.

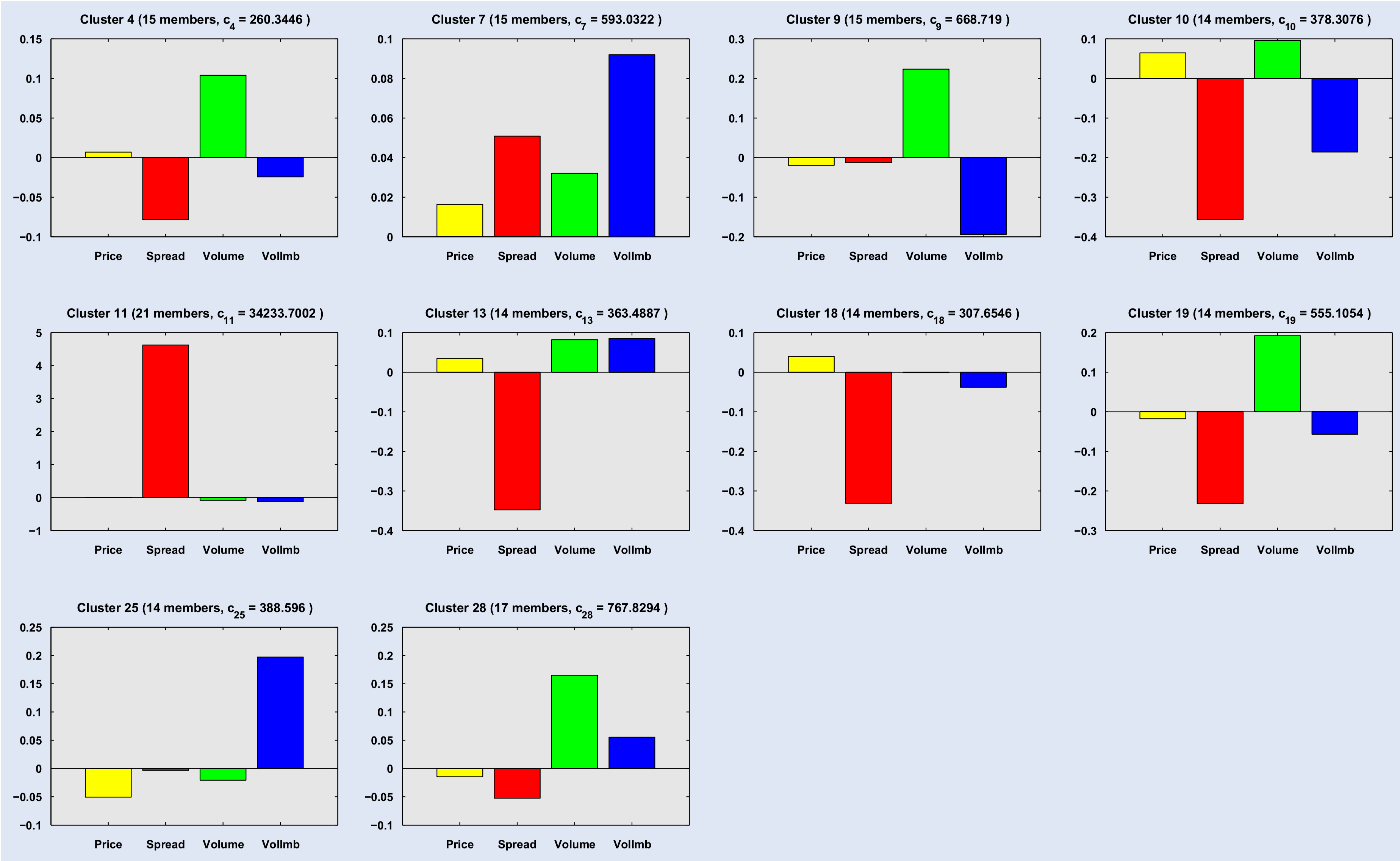

Figure 5. JSE TOP40 30-min cluster SSVs for the period 1 November 2012 to 30 November 2012. Each plot illustrates the average change in trade price, spread, trade volume and quote volume imbalance across member periods and stocks for each of the clusters with a size $\geq x_{\min}$ from the truncated power-law fit. Cluster size and intra-cluster correlation are shown in parentheses.

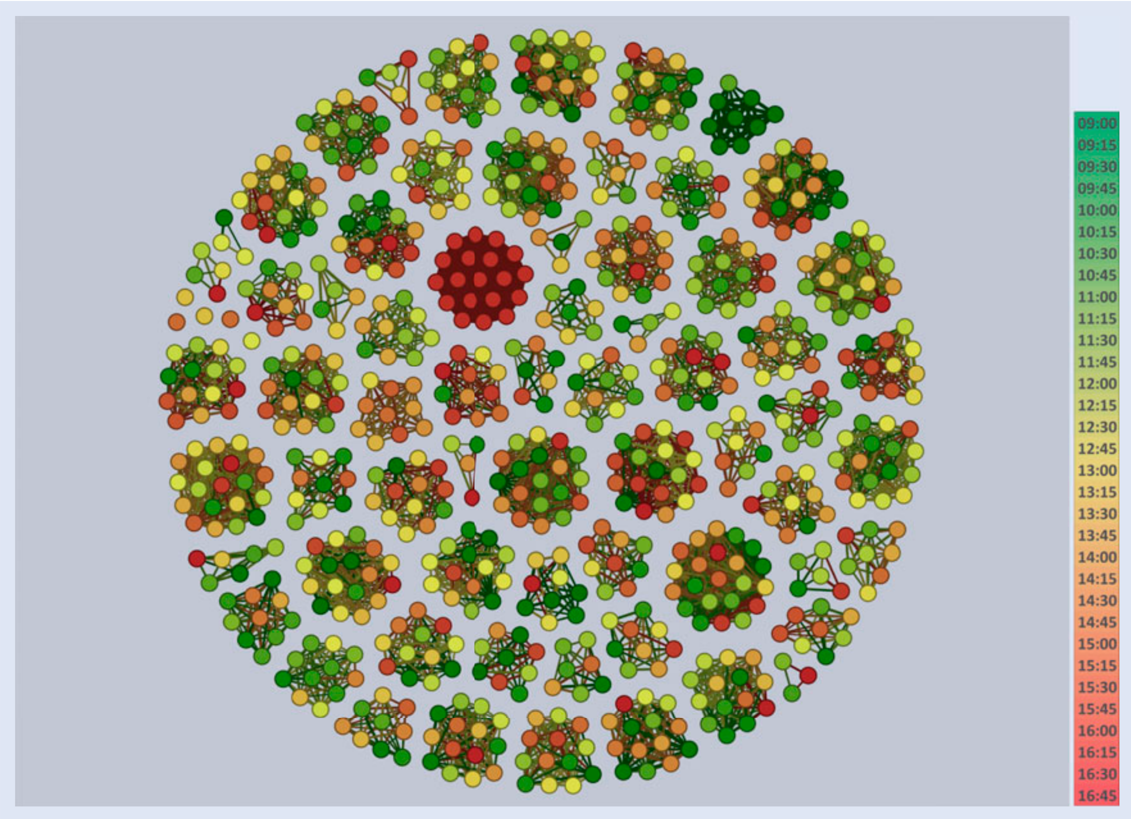

Figure 6. JSE TOP40 15-min temporal clusters for the period 1 November 2012 to 30 November 2012, representing 736 distinct periods. Each node represents a 15-min period during a trading day, with the colour shading indicating the time-of-day (Morning = green, Lunch = yellow, Afternoon = red) and node connectedness indicating cluster membership.

clusters from microstructure-based time correlations indicates that intraday dynamics may be reducible to a finite set of temporal states. Considering the time-of-day colour shading, we notice two clusters which exhibit market activity characteristics which coincide with morning and afternoon times. The dark green cluster refers to the first hour of the trading day (09:00 to 10:00), which incorporates opening auction and subsequent activity. We note that the South African equity market is strongly influenced by global market activity, in part due to local stocks being listed on multiple exchanges in the UK, USA, Europe and Australia (JSE 2014). During the period considered in this analysis, the UK market open occurred at 10:00 SAST and US market open at 15:30 SAST. The UK market open has a significant impact on local trading dynamics, with the 10:00 to 11:00 periods dispersing across clusters with no discernible time-of-day correlation. We note a contiguous dark orange cluster emerge from 15:00 to 16:00, as the US market starts to participate in local trading activity. This pattern of market activity broadly corroborates these exogenous market effects from global markets. Figure 3 shows the SSVs extracted from the significant states selected from figure 2. As discussed in section 7, we used the $x_{\min}$ statistic from the power-law fit to the tail distribution of cluster sizes to determine the significant states. For the 60-min periods, the most significant power-law fit was for cluster sizes ≥ 13, resulting in 6 significant states. The resulting SSVs are all relatively different, when considering the magnitude and direction of each of the average change in feature values. This ensures greater certainty in the state assignment of an online FV.

Table 5. Empirical 1-step transition probability matrix for 60-min states, based on identified temporal cluster configuration.

		$\mathbf{state}_{t+1}$					
		1	**2**	**3**	**4**	**5**	**6**
	1	0.13	0.49	0.32	0.00	0.06	0.00
	2	0.41	0.41	0.09	0.00	0.09	0.00
$\mathbf{state}_t$	**3**	0.00	0.00	0.00	0.52	0.05	0.43
	4	0.25	0.07	0.00	0.25	0.43	0.00
	5	0.32	0.59	0.05	0.05	0.00	0.00
	6	0.00	0.00	0.00	1.00	0.00	0.00

Note: State transitions with a probability > 0 are highlighted in green.

Figure 4 shows the temporal cluster configuration of 30-min periods. We see a larger number of states emerge as the granularity increases, with 60-min states being dissected based on finer-grained market activity. The dark green and dark orange contiguous morning and afternoon states still persist at this scale, although endogenous system characteristics begin to mask previously identified exogenous characteristics. We note that there is no defined hierarchy emerging, in that a set of 30-min clusters cannot be combined to form the 60-min clusters identified previously, further highlighting timescale-specific behaviour. Figure 5 shows the SSVs of significant states, based on the 10 clusters with a size ≥ 14.

Figure 6 shows the temporal cluster configuration of 15-min periods. We notice increasing time-of-day diversity in each of the identified clusters, further highlighting endogenous system

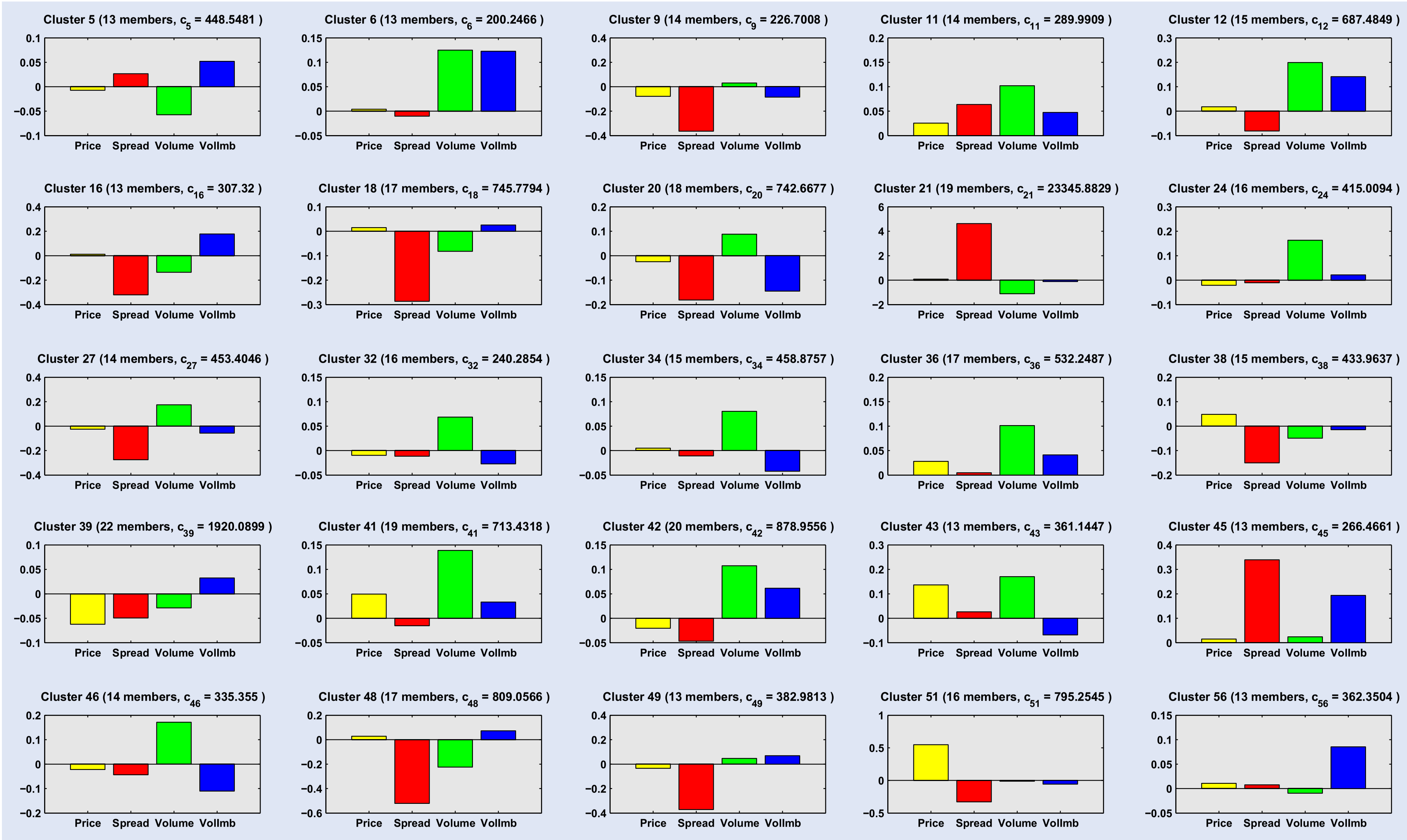

Figure 7. JSE TOP40 15-min cluster SSVs for the period 1 November 2012 to 30 November 2012. Each plot illustrates the average change in trade price, spread, trade volume and quote volume imbalance across member periods and stocks for each of the clusters with a size $\geq x_{\min}$ from the truncated power-law fit. Cluster size and intra-cluster correlation are shown in parentheses.

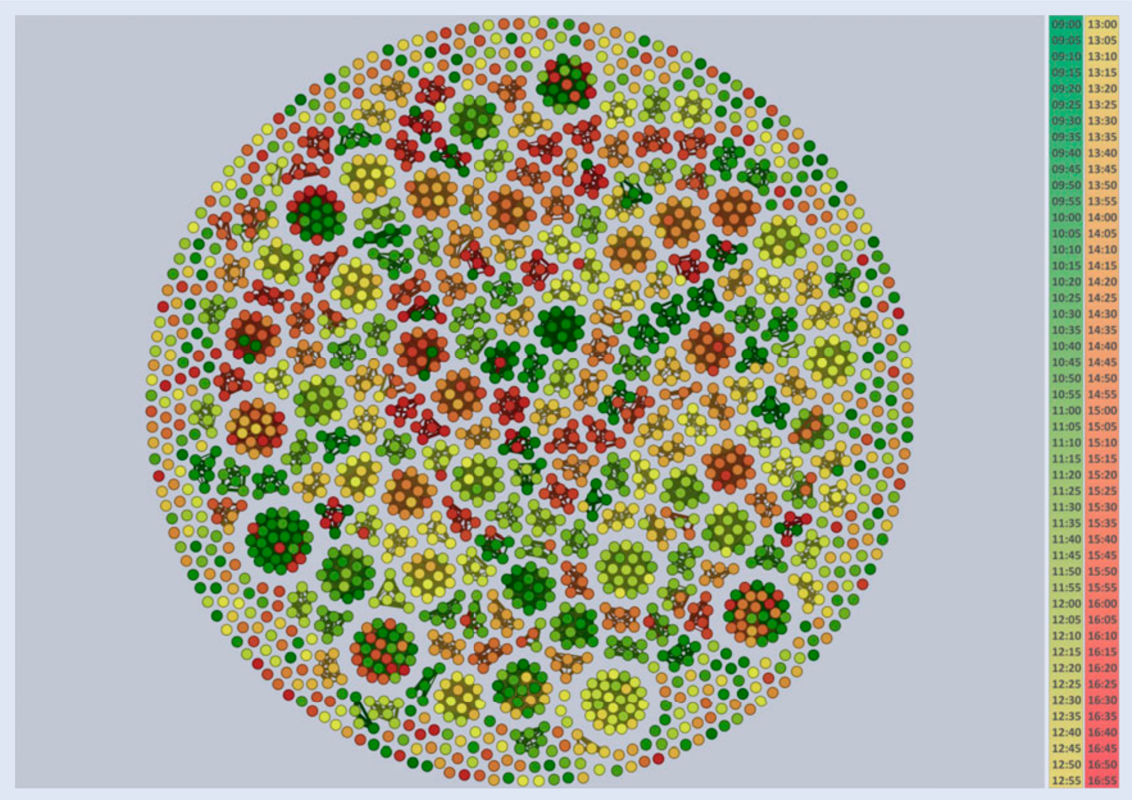

Figure 8. JSE TOP40 5-min temporal clusters for the period 1 November 2012 to 30 November 2012, representing 2208 distinct periods. Each node represents a 5-min period during a trading day, with the colour shading indicating the time-of-day (Morning = green, Lunch = yellow, Afternoon = red) and node connectedness indicating cluster membership.

Table 6. Empirical 1-step transition probability matrix for 30-min states, based on identified temporal cluster configuration.

		$\mathbf{state_{t+1}}$									
		1	**2**	**3**	**4**	**5**	**6**	**7**	**8**	**9**	**10**
	1	0.11	0.37	0.03	0.16	0.18	0.05	0.03	0.03	0.03	0.03
	2	0.07	0.04	0.35	0.06	0.04	0.10	0.17	0.10	0.04	0.01
	3	0.06	0.33	0.10	0.07	0.17	0.09	0.06	0.04	0.03	0.04
	4	0.05	0.08	0.26	0.03	0.21	0.18	0.00	0.13	0.03	0.03
$\mathbf{state_t}$	**5**	0.07	0.13	0.24	0.11	0.04	0.09	0.07	0.13	0.04	0.07
	6	0.10	0.21	0.10	0.03	0.14	0.03	0.00	0.17	0.10	0.10
	7	0.57	0.00	0.00	0.38	0.00	0.05	0.00	0.00	0.00	0.00
	8	0.13	0.23	0.16	0.16	0.13	0.03	0.06	0.06	0.03	0.00
	9	0.00	0.15	0.38	0.15	0.08	0.00	0.00	0.08	0.00	0.15
	10	0.00	0.36	0.21	0.07	0.29	0.00	0.00	0.07	0.00	0.00

Note: State transitions with a probability > 0 are highlighted in green.

activity. The red contiguous cluster is associated with the period from 16:30 to 16:45, suggesting a particular signature of market activity leading into the closing auction, which starts at 16:50. The UK- and US-related effects seem to have a weaker impact at this scale, with exchange-specific rules having a more dominant effect. As a result, we see a larger variety of SSVs in figure 7, some with similar profiles seen at the 30-min scale, but with a larger focus on magnitude rather than merely direction.

Figure 8 shows the temporal cluster configuration of 5-min periods. Here we see quite a different profile of system behaviour. There are a large number of singletons, which could be attributed to the amount of noise in the data at this scale, making it more difficult to discern significant structure. We notice an interesting time-of-day correlation with detected clusters, however broad periods (morning, lunch, afternoon) appear to have been dissected into contiguous blocks based on state-specific market activity. The 5-min timescale is starting to capture the effects of automated, rule-based trading agents which show quite a different characteristic signature. This further highlights the importance of studying market activity profiles at the scale at which you intend to participate.

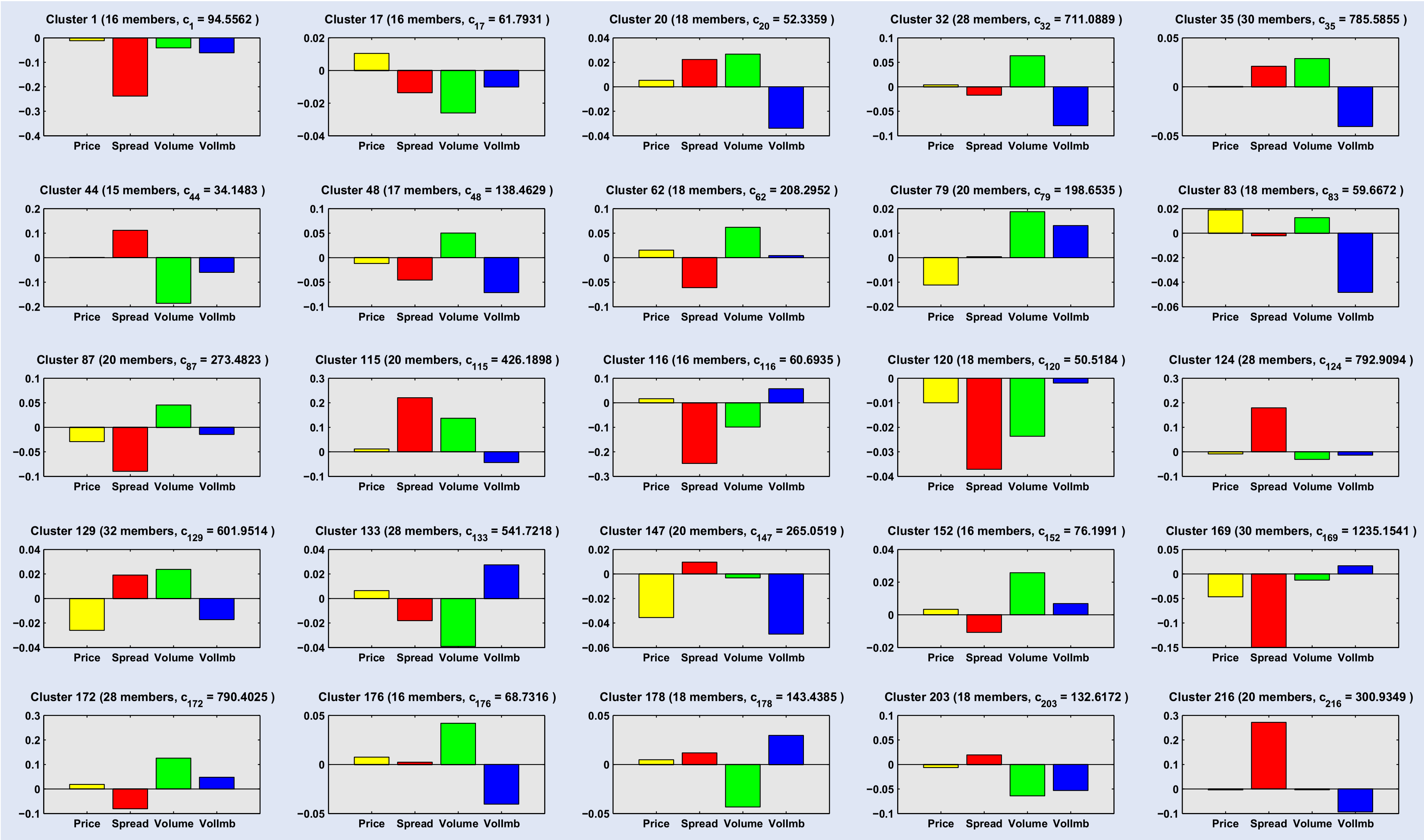

Figure 9. JSE TOP40 5-min cluster SSVs for the period 1 November 2012 to 30 November 2012. Each plot illustrates the average change in trade price, spread, trade volume and quote volume imbalance across member periods and stocks for each of the clusters with a size $\geq x_{\min}$ from the truncated power-law fit. Cluster size and intra-cluster correlation are shown in parentheses.

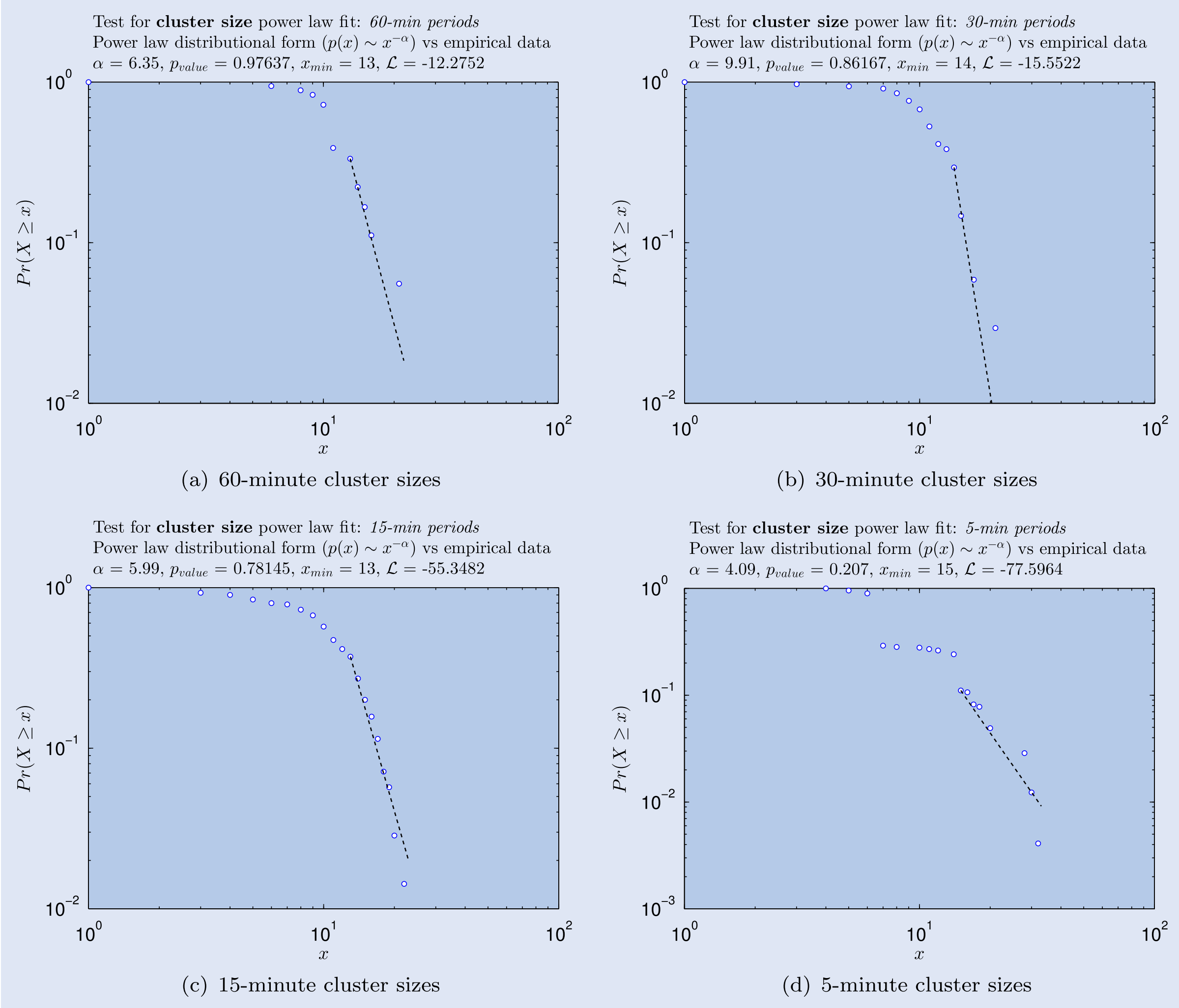

Figure 10. Testing conjecture of power law fit for varying time scale cluster sizes, applying the Clauset, Shalizi and Newman algorithm (Clauset *et al*. 2009). α indicates the scaling parameter of the proposed fit, p_{value} indicates the p-value from a Kolmogorov–Smirnov test for the goodness-of-fit of the proposed model to the data, $x_{\min}$ indicates the lower-bound for the power law fit and $\mathcal{L}$ is the log-likelihood of the data $(x \geq x_{\min})$ under the power law fit.

Table 7. Empirical 1-step transition probability matrix for 15-min states, based on identified temporal cluster configuration.

	state_{t+1}																								
	1	**2**	**3**	**4**	**5**	**6**	**7**	**8**	**9**	**10**	**11**	**12**	**13**	**14**	**15**	**16**	**17**	**18**	**19**	**20**	**21**	**22**	**23**	**24**	**25**
1	0.00	0.20	0.13	0.00	0.07	0.00	0.03	0.17	0.10	0.07	0.03	0.03	0.03	0.03	0.00	0.00	0.00	0.03	0.07	0.00	0.00	0.00	0.00	0.00	0.00
2	0.07	0.03	0.07	0.08	0.09	0.01	0.01	0.08	0.03	0.07	0.02	0.04	0.02	0.03	0.18	0.08	0.02	0.00	0.01	0.01	0.02	0.00	0.00	0.00	0.00
3	0.02	0.12	0.02	0.20	0.13	0.00	0.00	0.03	0.03	0.17	0.03	0.05	0.00	0.00	0.17	0.00	0.00	0.00	0.02	0.00	0.02	0.00	0.00	0.00	0.00
4	0.07	0.16	0.02	0.07	0.09	0.00	0.02	0.13	0.00	0.04	0.00	0.09	0.05	0.00	0.02	0.07	0.00	0.00	0.07	0.05	0.00	0.02	0.02	0.00	0.00
5	0.03	0.28	0.15	0.08	0.00	0.03	0.00	0.08	0.03	0.03	0.00	0.08	0.00	0.03	0.10	0.00	0.00	0.00	0.10	0.00	0.00	0.00	0.00	0.00	0.00
6	0.50	0.25	0.00	0.00	0.00	0.00	0.00	0.00	0.00	0.25	0.00	0.00	0.00	0.00	0.00	0.00	0.00	0.00	0.00	0.00	0.00	0.00	0.00	0.00	0.00
7	0.00	0.17	0.17	0.00	0.00	0.00	0.17	0.33	0.17	0.00	0.00	0.00	0.00	0.00	0.00	0.00	0.00	0.00	0.00	0.00	0.00	0.00	0.00	0.00	0.00
8	0.05	0.25	0.05	0.08	0.07	0.00	0.00	0.07	0.07	0.05	0.00	0.02	0.03	0.00	0.15	0.00	0.00	0.02	0.05	0.00	0.02	0.02	0.00	0.02	0.02
9	0.00	0.12	0.06	0.03	0.00	0.00	0.00	0.12	0.00	0.09	0.03	0.24	0.00	0.00	0.06	0.03	0.18	0.00	0.03	0.00	0.00	0.00	0.00	0.00	0.00
10	0.04	0.10	0.19	0.00	0.02	0.00	0.00	0.19	0.02	0.04	0.00	0.02	0.04	0.02	0.12	0.06	0.06	0.00	0.02	0.02	0.02	0.02	0.00	0.00	0.00
11	0.17	0.08	0.08	0.08	0.00	0.00	0.00	0.00	0.08	0.17	0.17	0.00	0.00	0.00	0.00	0.00	0.00	0.08	0.00	0.00	0.08	0.00	0.00	0.00	0.00
state_t 12	0.04	0.09	0.09	0.11	0.09	0.00	0.00	0.09	0.04	0.06	0.00	0.00	0.04	0.02	0.17	0.04	0.04	0.02	0.00	0.02	0.02	0.02	0.00	0.00	0.00
13	0.00	0.06	0.11	0.28	0.00	0.00	0.00	0.06	0.06	0.22	0.00	0.00	0.00	0.06	0.11	0.00	0.00	0.00	0.00	0.00	0.00	0.06	0.00	0.00	0.00
14	0.00	0.42	0.08	0.00	0.00	0.00	0.08	0.08	0.00	0.08	0.00	0.17	0.00	0.00	0.00	0.08	0.00	0.00	0.00	0.00	0.00	0.00	0.00	0.00	0.00
15	0.01	0.18	0.15	0.01	0.01	0.01	0.01	0.07	0.03	0.04	0.01	0.21	0.07	0.00	0.03	0.03	0.00	0.00	0.07	0.03	0.00	0.00	0.00	0.00	0.00
16	0.00	0.00	0.00	0.00	0.00	0.00	0.00	0.00	0.29	0.00	0.00	0.00	0.00	0.00	0.00	0.00	0.33	0.38	0.00	0.00	0.00	0.00	0.00	0.00	0.00
17	0.03	0.12	0.12	0.06	0.03	0.00	0.00	0.00	0.09	0.03	0.06	0.06	0.00	0.06	0.09	0.00	0.15	0.09	0.03	0.00	0.00	0.00	0.00	0.00	0.00
18	0.00	0.06	0.06	0.06	0.06	0.00	0.00	0.00	0.00	0.06	0.06	0.00	0.06	0.00	0.00	0.00	0.50	0.00	0.06	0.00	0.00	0.00	0.00	0.00	0.00
19	0.12	0.04	0.00	0.15	0.04	0.04	0.00	0.12	0.04	0.04	0.00	0.00	0.00	0.08	0.19	0.00	0.04	0.04	0.00	0.00	0.04	0.00	0.00	0.04	0.00
20	0.00	0.25	0.13	0.25	0.00	0.00	0.00	0.00	0.00	0.00	0.00	0.13	0.00	0.00	0.13	0.00	0.00	0.00	0.13	0.00	0.00	0.00	0.00	0.00	0.00
21	0.00	0.13	0.00	0.13	0.00	0.00	0.00	0.00	0.00	0.38	0.00	0.13	0.00	0.00	0.13	0.00	0.00	0.00	0.13	0.00	0.00	0.00	0.00	0.00	0.00
22	0.00	0.00	0.00	0.00	0.40	0.00	0.00	0.20	0.20	0.20	0.00	0.00	0.00	0.00	0.00	0.00	0.00	0.00	0.00	0.00	0.00	0.00	0.00	0.00	0.00
23	0.00	0.00	0.00	0.00	0.00	0.00	0.00	0.00	1.00	0.00	0.00	0.00	0.00	0.00	0.00	0.00	0.00	0.00	0.00	0.00	0.00	0.00	0.00	0.00	0.00
24	0.00	0.00	0.00	0.00	0.00	0.00	0.00	0.33	0.00	0.33	0.00	0.00	0.00	0.00	0.00	0.33	0.00	0.00	0.00	0.00	0.00	0.00	0.00	0.00	0.00
25	0.00	1.00	0.00	0.00	0.00	0.00	0.00	0.00	0.00	0.00	0.00	0.00	0.00	0.00	0.00	0.00	0.00	0.00	0.00	0.00	0.00	0.00	0.00	0.00	0.00

Note: State transitions with a probability $>$ 0 are highlighted in green.

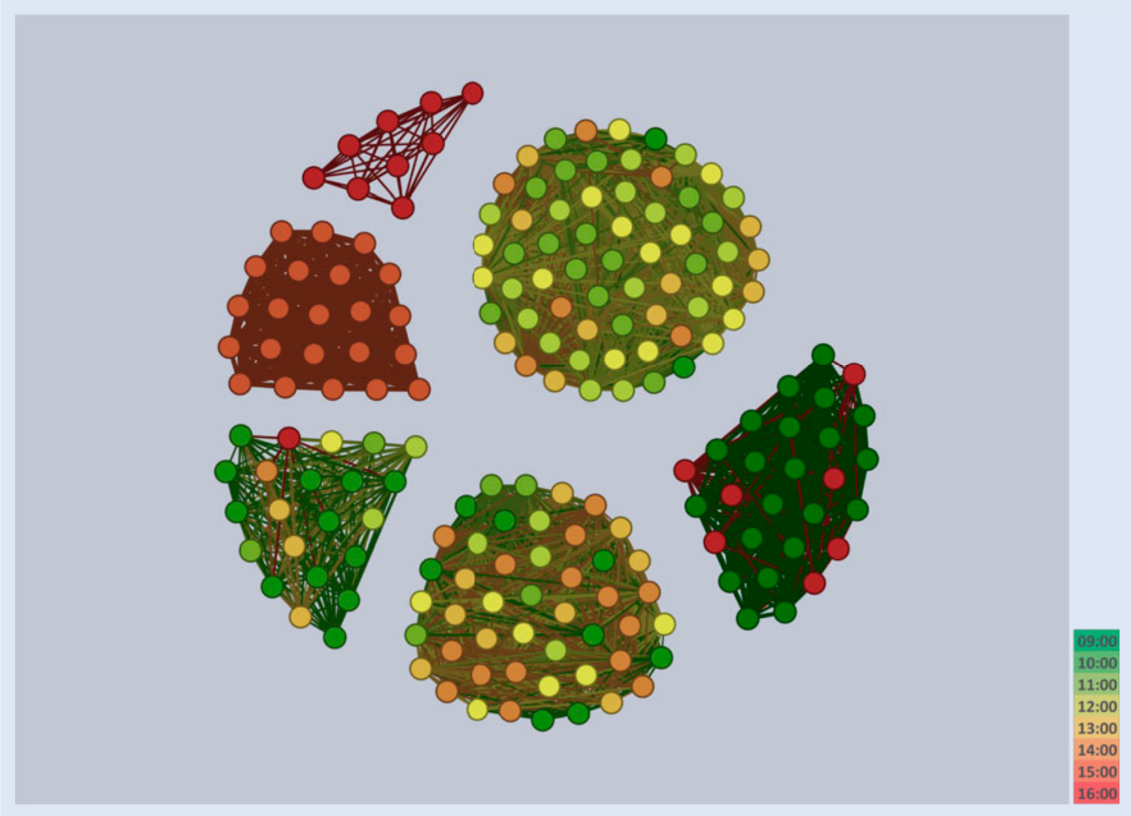

Figure 11. Estimated 60-min clusters using identified SSVs. The Euclidean distance is calculated between each temporal period's FV and the SSVs. Cluster index assignment is based on the SSV which yields the minimum distance.

Table 8. Empirical 1-step transition probability matrix for 5-min states, based on identified temporal cluster configuration.

	state_{t+1}																								
state_t	1	2	3	4	5	6	7	8	9	10	11	12	13	14	15	16	17	18	19	20	21	22	23	24	25
1	0.04	0.08	0.17	0.06	0.12	0.14	0.07	0.00	0.19	0.00	0.10	0.01	0.00	0.01	0.00	0.00	0.00	0.02	0.00	0.00	0.00	0.00	0.00	0.00	0.00
2	0.08	0.01	0.16	0.14	0.08	0.23	0.03	0.01	0.13	0.01	0.04	0.02	0.01	0.03	0.00	0.00	0.00	0.02	0.00	0.01	0.00	0.00	0.00	0.00	0.01
3	0.04	0.06	0.12	0.12	0.11	0.33	0.05	0.02	0.07	0.00	0.02	0.00	0.00	0.01	0.00	0.00	0.00	0.00	0.00	0.00	0.00	0.00	0.00	0.00	0.00
4	0.04	0.07	0.24	0.03	0.17	0.21	0.02	0.02	0.08	0.01	0.05	0.00	0.00	0.01	0.00	0.00	0.00	0.02	0.00	0.01	0.00	0.00	0.00	0.00	0.00
5	0.04	0.03	0.16	0.13	0.06	0.16	0.08	0.03	0.23	0.00	0.03	0.00	0.00	0.00	0.00	0.00	0.00	0.01	0.00	0.00	0.00	0.00	0.00	0.00	0.00
6	0.07	0.07	0.32	0.12	0.08	0.09	0.02	0.01	0.13	0.02	0.03	0.01	0.00	0.02	0.00	0.00	0.01	0.00	0.00	0.00	0.00	0.00	0.00	0.00	0.00
7	0.14	0.07	0.24	0.04	0.23	0.10	0.04	0.01	0.05	0.00	0.02	0.00	0.00	0.01	0.00	0.02	0.00	0.02	0.00	0.00	0.00	0.00	0.00	0.00	0.00
8	0.02	0.05	0.33	0.10	0.10	0.18	0.03	0.03	0.10	0.03	0.00	0.00	0.00	0.03	0.00	0.00	0.00	0.03	0.00	0.00	0.00	0.00	0.00	0.00	0.00
9	0.11	0.04	0.15	0.04	0.20	0.30	0.04	0.02	0.03	0.00	0.03	0.00	0.00	0.01	0.00	0.00	0.00	0.01	0.00	0.00	0.00	0.00	0.00	0.00	0.00
10	0.06	0.12	0.24	0.00	0.00	0.18	0.06	0.06	0.29	0.00	0.00	0.00	0.00	0.00	0.00	0.00	0.00	0.00	0.00	0.00	0.00	0.00	0.00	0.00	0.00
11	0.19	0.01	0.26	0.21	0.07	0.13	0.00	0.00	0.04	0.01	0.03	0.00	0.00	0.04	0.00	0.00	0.00	0.00	0.00	0.00	0.00	0.00	0.00	0.00	0.00
12	0.11	0.11	0.00	0.00	0.22	0.22	0.00	0.22	0.11	0.00	0.00	0.00	0.00	0.00	0.00	0.00	0.00	0.00	0.00	0.00	0.00	0.00	0.00	0.00	0.00
13	0.00	0.33	0.33	0.00	0.00	0.00	0.00	0.00	0.00	0.00	0.00	0.00	0.00	0.00	0.00	0.00	0.00	0.33	0.00	0.00	0.00	0.00	0.00	0.00	0.00
14	0.03	0.03	0.17	0.00	0.10	0.37	0.00	0.03	0.10	0.00	0.07	0.00	0.00	0.07	0.00	0.00	0.00	0.00	0.00	0.00	0.00	0.00	0.03	0.00	0.00
15	0.00	0.00	0.33	0.00	0.33	0.00	0.00	0.33	0.00	0.00	0.00	0.00	0.00	0.00	0.00	0.00	0.00	0.00	0.00	0.00	0.00	0.00	0.00	0.00	0.00
16	0.00	0.00	0.20	0.40	0.20	0.00	0.00	0.20	0.00	0.00	0.00	0.00	0.00	0.00	0.00	0.00	0.00	0.00	0.00	0.00	0.00	0.00	0.00	0.00	0.00
17	0.20	0.00	0.20	0.20	0.00	0.40	0.00	0.00	0.00	0.00	0.00	0.00	0.00	0.00	0.00	0.00	0.00	0.00	0.00	0.00	0.00	0.00	0.00	0.00	0.00
18	0.00	0.12	0.24	0.24	0.04	0.12	0.04	0.08	0.04	0.00	0.00	0.00	0.00	0.00	0.00	0.00	0.00	0.04	0.00	0.00	0.00	0.04	0.00	0.00	0.00
19	1.00	0.00	0.00	0.00	0.00	0.00	0.00	0.00	0.00	0.00	0.00	0.00	0.00	0.00	0.00	0.00	0.00	0.00	0.00	0.00	0.00	0.00	0.00	0.00	0.00
20	0.14	0.14	0.14	0.14	0.00	0.14	0.00	0.00	0.29	0.00	0.00	0.00	0.00	0.00	0.00	0.00	0.00	0.00	0.00	0.00	0.00	0.00	0.00	0.00	0.00
21	0.00	0.00	0.00	0.00	0.00	1.00	0.00	0.00	0.00	0.00	0.00	0.00	0.00	0.00	0.00	0.00	0.00	0.00	0.00	0.00	0.00	0.00	0.00	0.00	0.00
22	0.00	0.00	0.25	0.00	0.00	0.50	0.00	0.00	0.25	0.00	0.00	0.00	0.00	0.00	0.00	0.00	0.00	0.00	0.00	0.00	0.00	0.00	0.00	0.00	0.00
23	0.00	0.00	0.50	0.50	0.00	0.00	0.00	0.00	0.00	0.00	0.00	0.00	0.00	0.00	0.00	0.00	0.00	0.00	0.00	0.00	0.00	0.00	0.00	0.00	0.00
24	0.00	0.00	0.00	1.00	0.00	0.00	0.00	0.00	0.00	0.00	0.00	0.00	0.00	0.00	0.00	0.00	0.00	0.00	0.00	0.00	0.00	0.00	0.00	0.00	0.00
25	0.00	0.00	0.00	0.00	0.00	0.00	0.00	0.00	0.00	0.00	0.00	0.00	0.00	1.00	0.00	0.00	0.00	0.00	0.00	0.00	0.00	0.00	0.00	0.00	0.00

Note: State transitions with a probability $>$ 0 are highlighted in green.

Even when one considers the associated SSVs in figures 7 and 9, the 5-min and 15-min studies exhibit the same number of significant states using the power-law criterion; however, the combinations of direction and magnitude for the feature values are quite different.

Figure 10 illustrates the results of the power-law fits to the cluster size empirical distribution at each timescale. Each fit to the tail distribution exhibits a Kolmogorov–Smirnov p-value > 0.1 (assuming a null hypothesis of a power-law fit), suggesting a strong fit of the power-law functional form for the given scaling factor (α) and minimum size ($x_{\min}$) (Clauset *et al.* 2009). In addition, we note the α exponents are different for each of the timescales considered. This evidence of statistically significant power-law fits at each measured scale is consistent with the notion of financial markets as a complex adaptive system, and that the system is near criticality at

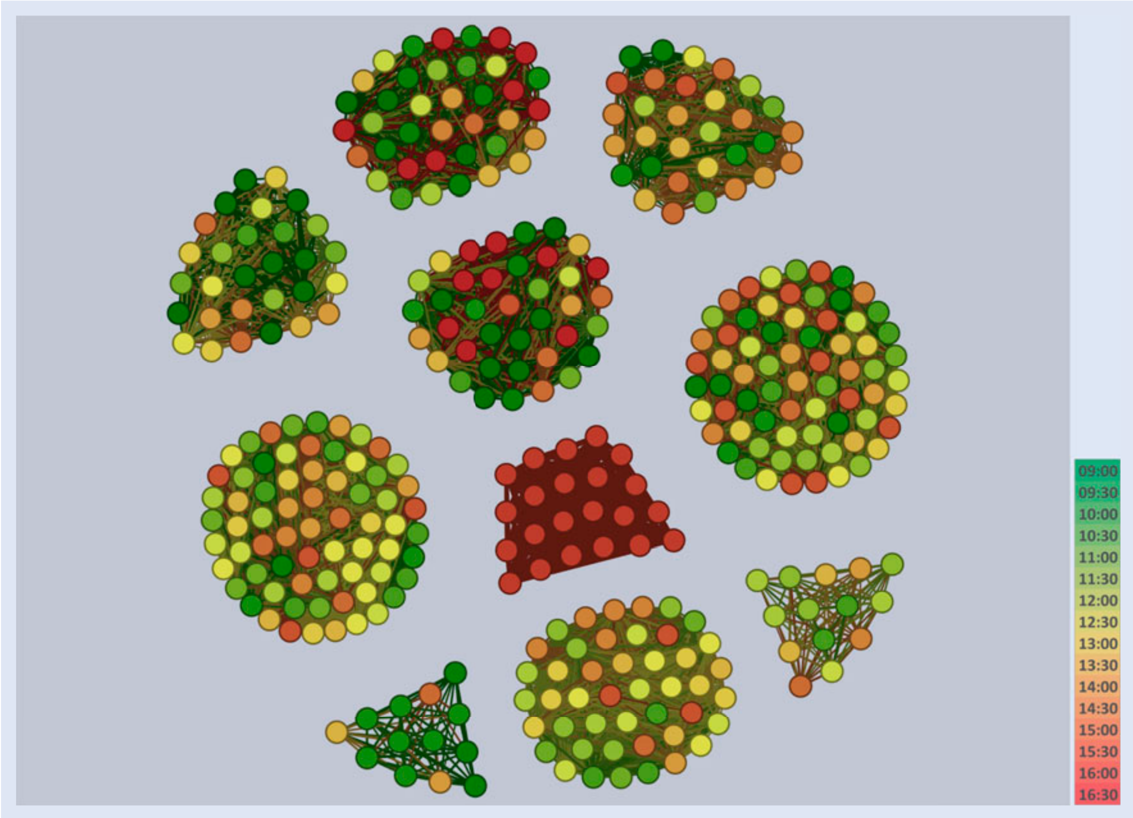

Figure 12. Estimated 30-min clusters using identified SSVs. The Euclidean distance is calculated between each temporal period's FV and the SSVs. Cluster index assignment is based on the SSV which yields the minimum distance.

each measured time scale (Mastromatteo and Marsili 2011). A further study should verify whether this suggests different universality classes of system behaviour at different timescales; however, these preliminary results do indicate the presence of some complex hierarchy of system behaviour, motivating the need for scale-specific temporal analysis.

Figure 11 shows the estimated 60-min cluster configuration for the same period (1 November 2012 to 30 November 2012), but where the distance of each period's FV to the identified SSVs is used as the criterion for state assignment. This is a simple in-sample test to determine whether the proposed scheme for online state assignment can discern the structure suggested by direct application of the clustering algorithm. By comparing figures 11 and 2, we notice that the online state assignment algorithm does recover the contiguous morning and afternoon states, but more broadly intuitively separates periods into: opening auction and early morning trading state, UK market open state, two lunch states, US market open state and a end-of-day/closing auction state. This completely captures the exogenous market effects, which is a strong validation for the approach. Table 5 shows an empirical 1-step transition probability matrix calculated from the states shown in figure 11, illustrating one potential application of this technique. The 1-step transitions show a particular preference, suggesting some predictability which can be exploited by trading agents. To be clear, the online assignment of a FV to a state means that we have developed a mechanism to *detect* which state we are currently in, using the prevailing set of SSVs. The transition matrix can be used and updated online, and for optimal planning in the domain.

Figures 12–14 and tables 6–8 show the estimated cluster configurations and transition probability matrices using the SSVs at the specified time scale. It is interesting to observe the dilution of the exogenous time-of-day effects as one approaches the 5-min scale.

Figure 15 illustrates the stability of the online state assignment algorithm out-of-sample. Given that the state assignment of an online FV is based on the minimum Euclidean distance to predetermined SSVs, we compute the *best match* distance for each of the FVs in a sample and use a boxplot to visualize the empirical distribution. This paper proposes offline estimation of SSVs used for online state detection. The online cluster configurations shown in figures 11–14 use FVs from the *ex-ante* period, i.e. the same period used to estimate the SSVs. It is prudent to determine whether state assignment using out-of-sample (*ex-post*) FVs deviate significantly from in-sample assignment, and gauge the out-of-sample efficacy of the SSVs before re-estimation is necessary. Given the computation times shown in section 5, in practice one could estimate the SSVs overnight for each trading day. We have considered SSVs estimated from the period 1 November 2012 to 30 November 2012, and compared the resulting online states from the *ex-ante* period (1 November 2012 to 30 November 2012) with states from an *ex-post* period (3 December 2012 to 7 December 2012, one week after SSV estimation). From these results, it appears that 60-min states cannot be reliably determined *ex-post* using the online detection algorithm, given the observed higher range of *best match* Euclidean distances. The 30-min, 15-min and 5-min timescales all exhibit acceptable *ex-post best match* distances, with the exception of a few

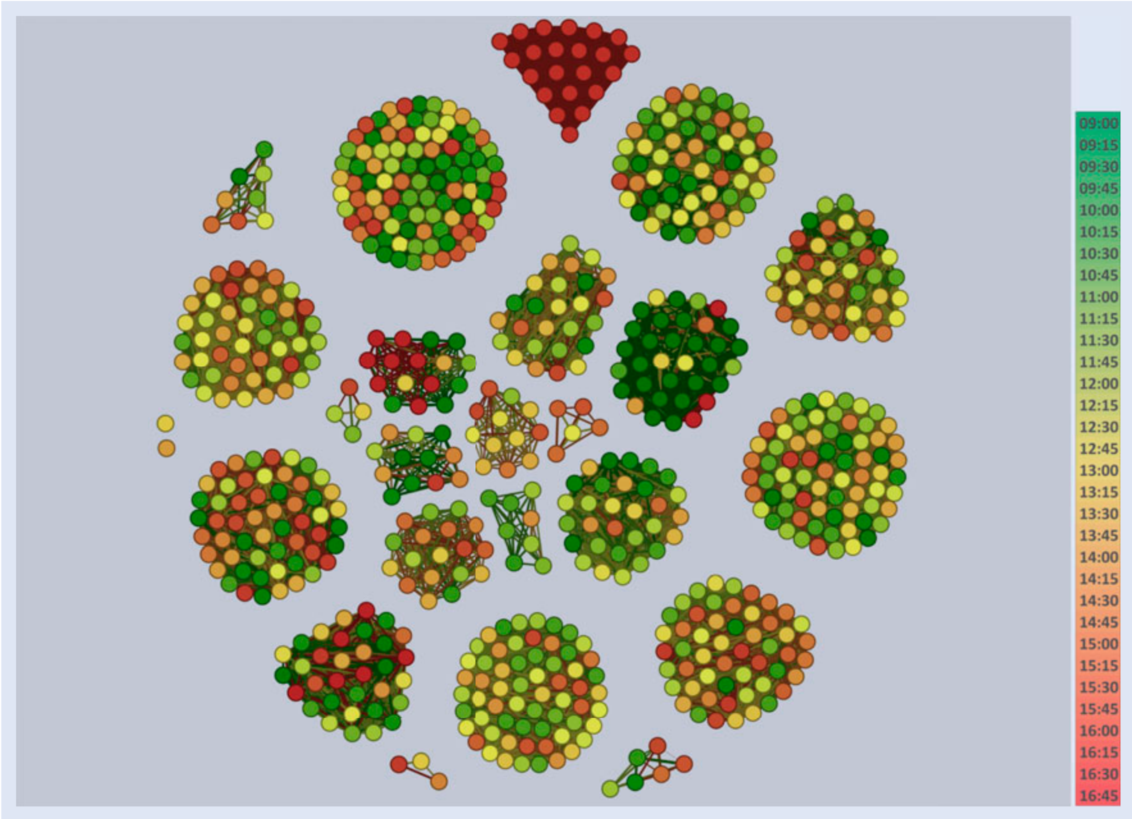

Figure 13. Estimated 15-min clusters using identified SSVs. The Euclidean distance is calculated between each temporal period's FV and the SSVs. Cluster index assignment is based on the SSV which yields the minimum distance.

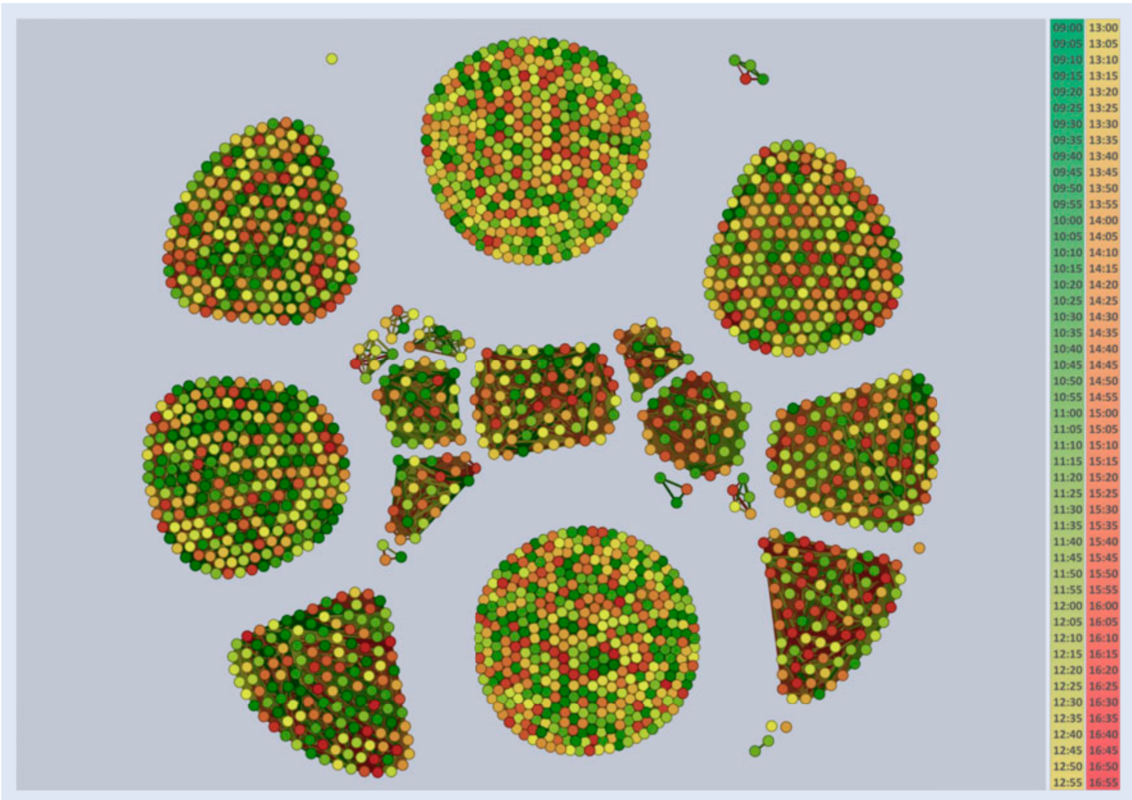

Figure 14. Estimated 5-min clusters using identified SSVs. The Euclidean distance is calculated between each temporal period's FV and the SSVs. Cluster index assignment is based on the SSV which yields the minimum distance.

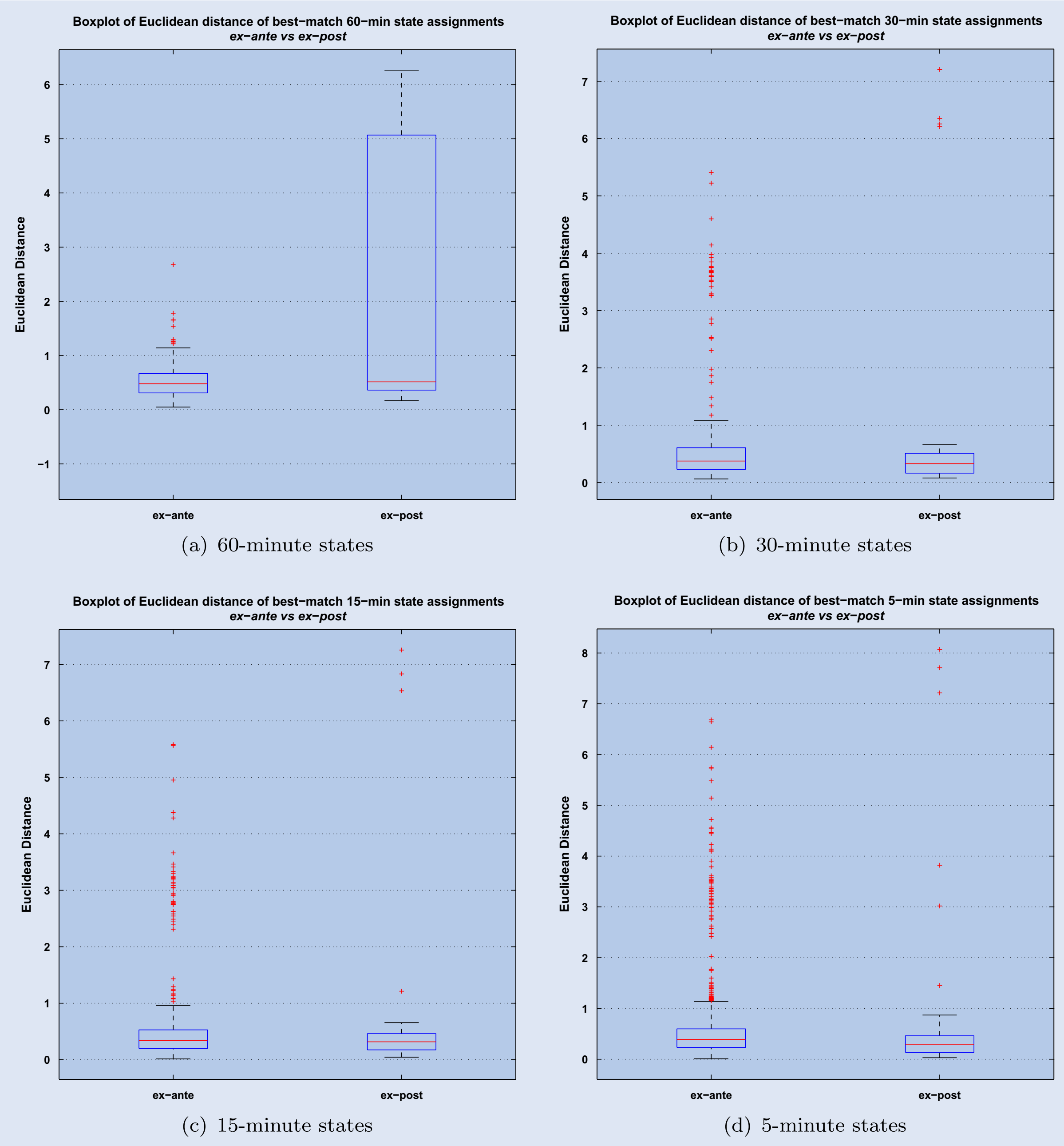

(a) 60-minute states (b) 30-minute states (c) 15-minute states (d) 5-minute states

Figure 15. Measuring the stability of the online state assignment algorithm out-of-sample. Given that the state assignment of an online FV is based on the minimum Euclidean distance to predetermined SSVs, we compute the *best match* distance for each of the FVs in a sample and use a boxplot to visualize the empirical distribution. In this figure, we compare the *ex-ante* (1 November 2012 to 30 November 2012, same period used for SSV estimation) and *ex-post* (3 December 2012 to 7 December 2012, one week after SSV estimation window) periods.

outliers. From these preliminary results, it appears that the algorithm can be used to reliably determine 30-min, 15-min and 5-min states for a relatively short *ex-post* period following SSV estimation. A more robust study should consider the precise half-life of the SSVs, but given the relatively fast computation time, this is unlikely to be a practical concern.

9. Conclusion

In this paper, we have outlined a novel approach for the unsupervised detection of intraday temporal market states at varying timescales, as well as a proposed mechanism for significant state selection and online state estimation. Using the maximum likelihood approach of Giada and Marsili (2001), we show that the technique can be used to cluster temporal periods as objects based on market microstructure feature performance. A high-speed PGA was used for cluster detection, with a computation time conducive to overnight or even intraday calibration of market states. A study of temporal cluster configurations and power-law fits to 60-min, 30-min, 15-min and 5-min timescales revealed scale-specific system behaviour, motivating the need for scale-specific state space reduction for optimal planning of participating trading agents. The proposed scheme for online state detection suggested the use of SSVs to capture the market activity signature of each identified state, with a simple distance metric of the prevailing FV to determine the state index. We showed that the online state detection scheme can be used to enumerate and update 1-step transition probability matrices, which can be used for optimal planning in the high-frequency trading domain. We considered the stability of the algorithm *ex-post* and found that we could reliably determine 30-min, 15-min and 5-min states using the proposed algorithm, whereas 60-min states were less stable.

While this paper demonstrates a feasible framework for temporal state detection, further research should consider a longer term study to determine the stability of identified states and explore alternative propositions for features, state signature extraction and online detection. In the South African equity market, the impact of significant infrastructure changes (e.g. exchange server migration, fee model modifications, co-located trading servers) on temporal system behaviour can be considered.

Acknowledgements

The conclusions herein are due to the authors and the NRF accepts no liability in this regard. We also thank the Fields Institute for Research in Mathematical Sciences and the University of Toronto for hosting the first author while much of the work for this paper was completed.

Disclosure statement

No potential conflict of interest was reported by the authors.

Funding

This work is based on the research supported in part by the National Research Foundation of South Africa [grant number 89250].

ORCID

D. Hendricks http://orcid.org/0000-0003-4523-6386
T. Gebbie http://orcid.org/0000-0002-4061-2621
D. Wilcox http://orcid.org/0000-0003-1832-3601

References

Abergel, F. and Jedidi, A., Long time behaviour of a hawkes process-based limit order book. Working Paper, 2015. Available online at SSRN: http://ssrn.com/abstract=2575498.

Adi, A., Botzer, D., Nechushtai, G. and Sharon, G., Complex event processing for financial services. In *Proceedings from the IEEE Services Computing Workshops*, Chicago, IL, pp. 7–12, 2006.

Arthur, W., Complexity in economic and financial markets. *Complexity*, 1995, **1**(1), 20–25.

Arthur, W., Holland, J., LeBaron, B., Palmer, R. and Taylor, P., Asset pricing under endogenous expectations in an artificial stock market. In *The Economy as an Evolving Complex System*, edited by W.B. Arthur, S.N. Durlauf and D.A. Lane, Vol. 2, pp. 15–44, 1997 (Westview Press: Boulder, CO).

Bacry, E., Mastromatteo, I. and Muzy, J., Hawkes processes in finance. *Market Micro. Liquid.*, 2015, **1**(1), 1550005.

Baldovin, F., Camana, F., Caporin, M., Caraglio, M. and Stella, A., Ensemble properties of high-frequency data and intraday trading rules. *Quant. Finance*, 2015, **15**(2), 231–245.

Bastian, M., Heymann, S. and Jacomy, M., Gephi: An open source software for exploring and manipulating networks. In *Proceedings from the International AAAI Conference on Weblogs and Social Media*, San Jose, CA, 2009.

Bauke, H., Parameter estimation for power-law distributions by maximum likelihood methods. *Eur. Phys. J. B*, 2007, **58**(2), 167–173.

Biais, L., Glosten, C. and Spatt, C., Market microstructure: A survey of microfoundations, empirical results, and policy implications. *J. Financ. Markets*, 2005, **8**(2), 217–264.

Blatt, M., Wiseman, S. and Domany, E., Superparamagnetic clustering of data. *Phys. Rev. Lett.*, 1996, **76**(18), 3251–3254.

Blatt, M., Wiseman, S. and Domany, E., Data clustering using a model granular magnet. *Neural Comput.*, 1997, **9**, 1805–1842.

Brock, W., Pathways to randomness in the economy: Emergent nonlinearity and chaos in economics and finance. *Estud. Econ.*, 1993, **8**, 3–55.

Cieslakiewicz, D., Unsupervised asset cluster analysis implemented with parallel genetic algorithms on the Nvidia CUDA platform. Master's Thesis, University of the Witwatersrand, 2014.

Clauset, A., Shalizi, C. and Newman, M., Power-law distributions in empirical data. *SIAM Rev.*, 2009, **51**(4), 661–703.

Cont, R. and Tankov, P., *Financial Modelling with Jump Processes*, CRC Financial Mathematics Series, 2004 (Chapman & Hall: London).

Dacorogna, M., Gauvreau, C., Muller, U., Olsen, R. and Pictet, O., Changing time scale for short-term forecasting in financial markets. *J. Forecasting*, 1996, **15**, 203–227.

Derman, E., The perception of time, risk and return during periods of speculation. *Quant. Finance*, 2002, **2**, 282–296.

Easley, D., López de Prado, M. and O'Hara, M., The volume clock: Insights into the high-frequency paradigm (digest summary). *J. Portfolio Manage.*, 2012, **39**(1), 19–29.

Emmert-Streib, F. and Dehmer, M., Influence of the time scale on the construction of financial networks. *PLoS ONE*, 2010, **5**(9), e12884.

Engle, R. and Russell, J., Autoregressive conditional duration: A new model for irregularly spaced transaction data. *Econometrica*, 1998, **66**, 1127–1162.

Fruchterman, T. and Reingold, E., Graph drawing by force-directed placement. *Software Pract. Exper.*, 1991, **21**(11), 1129–1164.

Gabaix, X., Gopikrishnan, P., Plerou, V. and Stanley, H., A theory of power-law distributions in financial market fluctuations. *Nature*, 2003, **423**(6937), 267–270.

Garman, M., Market microstructure. *J. Financ. Econ.*, 1976, **3**, 257–275.

Gençay, R., Gradojevic, N., Selçuk, F. and Whitcher, B., Asymmetry of information flow between volatilities across time scales. *Quant. Finance*, 2010, **10**(8), 895–915.

Giada, L. and Marsili, M., Data clustering and noise undressing of correlation matrices. *Phys. Rev. E*, 2001, **63**(1), 061101.

Hasbrouck, J., Trades, quotes, inventories and information. *J. Financ. Econ.*, 1988, **22**, 229–252.

Hasbrouck, J., Measuring the information content of stock trades. *J. Finance*, 1991, **46**, 179–207.

Hendricks, D., Gebbie, T. and Wilcox, D., High-speed detection of emergent market clustering via an unsupervised parallel genetic algorithm. *S. Afr. J. Sci.*, 2016, **112**(1/2).

Hinton, G., Learning multiple layers of representation. *Trends Cogn. Sci.*, 2007, **11**(10), 428–434.

Hommes, C., Financial markets as nonlinear adaptive evolutionary systems. *Quant. Finance*, 2001, **1**(1), 149–167.

JSE, Dual-listed companies, 2014. Available online at: http://www.jse.co.za/how-tolist/mainboard/dual-listed-companies.aspx (accessed 8 March 2014).

JSE, Market data – Equities, derivatives and interest rate products price list, 2015. Available online at: https://www.jse.co.za/content/JSEPricingItems/JSE%20Equities%20Derivatives%20and%20Interest%20Rate%20Products%20Price%20List%202016.pdf (accessed 13 July 2015).

Kullmann, L., Kertész, J. and Mantegnae, R., Identification of clusters of companies in stock indices via potts super-paramagnetic

transitions. Working Paper, 2000. Available online at arXiv: http://arxiv.org/abs/cond-mat/0002238.
Large, J., Measuring the resiliency of an electronic limit order book. *J. Financ. Markets*, 2000, **10**, 1–25.
Madhavan, A., Market microstructure: A survey. *J. Financ. Markets*, 2000, **3**(3), 205–258.
Marsili, M., Dissecting financial markets: Sectors and states. *Quant. Finance*, 2002, **2**(4), 297–302.
Mastromatteo, I. and Marsili, M., On the criticality of inferred models. *J. Stat. Mech.: Theory Exper.*, 2011, **2011**(10), P10012.
McLachlan, G., Peel, D. and Whiten, W., Maximum likelihood clustering via normal mixture models. *Signal Process.: Image Commun.*, 1996, **8**(2), 105–111.
McNeil, A., Frey, R. and Embrechts, P., *Quantitative Risk Management: Concepts, Techniques and Tools*, Princeton Series in Finance, 2015 (Princeton University Press: Princeton, NJ).
Müller, U., Dacorogna, M., Davé, R., Pictet, O.V., Olsen, R. and Ward, J., *Fractals and Intrinsic Time – A Challenge to Econometricians*, 1995 (Zurich: Olsen and Associates).
Mungan, M. and Ramasco, J., Stability of maximum-likelihood-based clustering methods: Exploring the backbone of classifications. *J. Stat. Mech.: Theory Exper.*, 2010, **4**, P04028.
Noh, J., A model for correlations in stock markets. *Phys. Rev. E.*, 2000, **61**, 5981.
O'Hara, M., *Market Microstructure Theory*, 1998 (Blackwell: Hoboken, NJ).
Patterson, D. and Hennessy, J., *Computer Organization and Design: The Hardware/Software Interface*, 5th ed., 2013 (Morgan Kaufmann: Burlington, MA).
Toke, I. and Pomponio, F., Modelling trades-through in a limit order book using Hawkes processes. *Economics*, 2012, **6**(22), 1–23.
Wang, S. and Swendsen, R., Cluster monte carlo algorithms. *Physica A*, 1990, **167**(565), 565–579.
Wilcox, D. and Gebbie, T., Hierarchical causality in financial economics. Working Paper, 2014. Available online at SSRN: http://ssrn.com/abstract=2544327.
Wiseman, S., Blatt, M. and Domany, E., Superparamagnetic clustering of data. *Phys. Rev. E*, 1998, **57**, 37–67.
Zhang, L., Mykland, P. and Aït-Sahalia, Y., A tale of two time scales: Determining integrated volatility with noisy high-frequency data. *J. Am. Stat. Assoc.*, 2005, **100**(472), 1394–1411.

Appendix 1. The Noh–Giada–Marsili coupling parameters

According to Noh (2000), the generative model of the price associated with the ith stock can be written as

$$X_i(t) = g_{s_i}\eta_{s_i} + \sqrt{1-g_{s_i}^2}\epsilon_i, \tag{A1}$$

where the cluster-related influences are driven by η_{s_i} and the stock-specific influences by ϵ_i. Both innovations are treated as Gaussian random variables with unit variance and zero mean.† The relative contribution is controlled by the intra-cluster coupling parameter g_{s_i}. The Noh–Giada–Marsili model encodes the idea that stocks which have something in common belong in the same cluster. This comes with the caveat that stock membership in clusters is mutually exclusive and intra-cluster correlations are positive.

From equation (A1), we compute the covariance for the ith and jth stocks

$$\mathrm{E}[X_i(t)X_j(t)] = g_{s_i}^2\mathrm{E}[\eta_{s_i}\eta_{s_j}] + (1-g_{s_i}^2)\mathrm{E}[\epsilon_i\epsilon_j]. \tag{A4}$$

Using the assumption of unit variance and zero mean for both the shared component (η_{s_i}) and stock component (ϵ_i) processes, the correlation between stock i and j is given by

$$C_{ij} = g_{s_i}^2\delta_{s_is_j} + (1-g_{s_i}^2)\delta_{ij}. \tag{A5}$$

The following cluster relations can be derived, where n_s is the index of stock in the sth cluster and c_s is the internal correlation of the sth cluster, given that clusters are mutually exclusive

$$n_s = \sum_{i=1}^{N}\delta_{s_is}, \quad c_s = \sum_{i,j=1}^{N} C_{ij}\delta_{s_is}\delta_{s_js}. \tag{A6}$$

From equation (A5), for $s_i = s_j = s$, we have $C_{ij} \approx g_s^2$ (Giada and Marsili 2001). We can multiply both sides of equation (A5) by $\delta_{s_is}\delta_{s_js}$ and sum over all i and j to find

$$\sum_{i,j} C_{ij}\delta_{s_is}\delta_{s_js} = \sum_{i,j} g_{s_i}^2\delta_{s_is_j}\delta_{s_is}\delta_{s_js} + \sum_{i,j}(1-g_{s_i}^2)\delta_{ij}\delta_{s_is}\delta_{s_js}. \tag{A7}$$

To sum out the delta functions over the clusters and stocks from

$$\sum_{i,j} C_{ij}\delta_{s_is}\delta_{s_js} = \sum_i\left(g_{s_i}^2\delta_{s_is}\sum_j\delta_{s_is_j}\delta_{s_js}\right) + \sum_i\left((1-g_{s_i}^2)\delta_{s_is}\sum_j\delta_{ij}\delta_{s_js}\right), \tag{A8}$$

we use that $\sum_j\delta_{ij}\delta_{s_is} = \delta_{s_is}$, $\sum_j\delta_{s_is_j}\delta_{s_js} = n_s\delta_{s_is}$ and $\sum_i\delta_{s_is}^2 = \sum_i\delta_{s_is}$ to find

$$\sum_{i,j} C_{ij}\delta_{s_is}\delta_{s_js} = g_s^2 n_s\sum_i\delta_{s_is} + (1-g_s^2)\sum_i\delta_{s_is}. \tag{A9}$$

By combining equations (A6) and (A9), we get

$$c_s = g_s^2 n_s^2 + (1-g_s^2)n_s = g_s^2(n_s^2-n_s) - n_s. \tag{A10}$$

This is can be rearranged to finally obtain an expression for the intra-cluster coupling parameter for cluster s,

$$g_s = \sqrt{\frac{c_s-n_s}{n_s^2-n_s}}. \tag{A11}$$

Appendix 2. The Noh–Giada–Marsili likelihood function

We evaluate the probability of the data satisfying the model by using the multiplicative property of probabilities,

$$P(X_1(1),\ldots,X_N(D)) = \prod_{d=1}^{D}\prod_{i=1}^{N}P(X_i(d)). \tag{B1}$$

The probability of being in a given state that satisfies the model is given as a delta function, such that we sum over all N stocks and all D features (date-times), taking expectations $\langle\ldots\rangle_{\eta,\epsilon}$ over the random processes associated with the stock-specific noise and the cluster-specific noise

$$P = \prod_{d=1}^{D}\left\langle\prod_{i=1}^{N}\delta\left(X_i(d) - (g_{s_i}\eta_{s_i} + \sqrt{1-g_{s_i}^2}\epsilon_i)\right)\right\rangle_{\eta,\epsilon}. \tag{B2}$$

†This form of the price model ensures that the self correlation of a stock is one and independent of the cluster coupling. This can be seen by computing the self correlation $E[x_i^2]$ and using that clusters and stock unique process are unit variance zero mean processes

$$\mathrm{E}\left[\left(g_{s_i}\eta_{s_i} + \sqrt{1-g_{s_i}^2}\epsilon_i\right)^2\right] = g_{s_i}^2 + (1-g_{s_i}^2) = 1. \tag{A2}$$

This is not a unique choice, another possible choice often used is

$$\mathrm{E}\left[\left(\frac{\sqrt{g_{s_i}}}{\sqrt{1+g_{s_i}}}\eta_{s_i} + \frac{1}{\sqrt{1+g_{s_i}}}\epsilon_i\right)^2\right] = \frac{1+g_{s_i}}{1+g_{s_i}} = 1. \tag{A3}$$

This takes on the form

$$P = \prod_{d=1}^{D} \prod_{i=1}^{N} \int \mathrm{d}\epsilon_i \mathrm{d}\eta_{s_i}$$
$$\times \exp\left[-\frac{1}{2}\sum_{k}^{N} \epsilon_k \delta_{ki}\epsilon_i - \frac{1}{2}\sum_{p,q}^{N} \eta_{s_p}\eta_{s_q}\delta_{s_p s_i}\delta_{s_q s_i}\right] \tag{B3}$$
$$\times \delta\left(X_i(d) - g_{s_i}\eta_{s_i} - \sqrt{1-g_{s_i}^2}\epsilon_i\right). \tag{B4}$$

This is simplified to the following form, where the sum over i stocks is converted to sums of the clusters s and the n_s stocks in each cluster

$$P = \prod_{s=1}^{S} \prod_{d=1}^{D} \int \mathrm{d}\eta_s e^{-\frac{1}{2}\eta_s^2} \times \prod_{i\in s}^{n_s} \int \mathrm{d}\epsilon_i \exp\left[-\frac{1}{2}\epsilon_i^2\right] \delta\left(X_i(d) - g_s\eta_s - \sqrt{1-g_s^2}\epsilon_i\right). \tag{B5}$$

The Gaussian integral over the delta function is evaluated relative to the ϵ_i's, using that $\prod \int f(x)\delta(ax - x_0) = \prod \frac{1}{|a|} f(x_0/a)$ over the n_s delta functions,

$$P = \prod_{s=1}^{S} \prod_{d=1}^{D} \int \frac{\mathrm{d}\eta_s}{(1-g_s^2)^{\frac{n_s}{2}}} e^{-\frac{1}{2}\eta_s^2} \times \prod_{i\in s}^{n_s} \exp\left[-\frac{1}{2}\frac{(g_s\eta_s - X_i)^2}{1-g_s^2}\right]. \tag{B6}$$

Expanding out the integrand and using $\prod_i e_i^A = e^{\sum_i A_i}$,

$$P = \prod_{s=1}^{S} \prod_{d=1}^{D} \int \frac{\mathrm{d}\eta_s}{(1-g_s^2)^{\frac{n_s}{2}}} \times \exp\left[-\frac{1}{2}\eta_s^2 - \frac{1}{2}\sum_{i\in s}^{n_s} \frac{(g_s^2\eta_s^2 - 2g_s\eta_s X_i + X_i^2)}{1-g_s^2}\right] \tag{B7}$$

Expanding out the sum terms and evaluating where possible

$$P = \prod_{s=1}^{S} \prod_{d=1}^{D} \int \frac{\mathrm{d}\eta_s}{(1-g_s^2)^{\frac{n_s}{2}}} \times \exp\left[-\frac{1}{2}\eta_s^2 - \frac{1}{2}\frac{n_s g_s^2 \eta_s^2}{1-g_s^2} \frac{g_s\eta_s}{1-g_s^2}\sum_{i\in s}^{n_s} X_i - \frac{1}{2}\frac{1}{1-g_s^2}\sum_{i\in s}^{n_s} X_i^2\right]. \tag{B8}$$

This can be further simplified to

$$P = \prod_{s=1}^{S} \prod_{d=1}^{D} \int \frac{\mathrm{d}\eta_s}{(1-g_s^2)^{\frac{n_s}{2}}} \times \exp\left[-\frac{1}{2}\frac{1-g_s^2 + n_s g_s^2}{1-g_s^2}\eta_s^2 \frac{g_s\eta_s}{1-g_s^2}\sum_{i\in s}^{n_s} X_i - \frac{1}{2}\frac{1}{1-g_s^2}\sum_{i\in s}^{n_s} X_i^2\right]. \tag{B9}$$

We now evaluate the Gaussian integral using that $\int e^{-x^2}\mathrm{d}x = \sqrt{\pi/2}$ and hence that $\int e^{-ax^2+bx}\mathrm{d}x = \frac{\pi}{2a} e^{\frac{b^2}{4a}}$

$$P = \prod_{s=1}^{S} \prod_{d=1}^{D} \frac{\sqrt{\pi}}{(1-g_s^2)^{\frac{n_s}{2}}} \frac{(1-g_s^2)^{\frac{1}{2}}}{(n_s g_s^2 + (1-g_s^2))^{\frac{1}{2}}} \tag{B10}$$
$$\times \exp\left[\frac{g_s^2}{2(n_s g_s^2 + (1-g_s^2))(1-g_s^2)} (\sum_{i\in s}^{n_s} X_i)^2\right] \tag{B11}$$
$$\times \exp\left[-\frac{1}{2}\frac{1}{1-g_s^2}\sum_{i\in s}^{n_s} X_i^2\right]. \tag{B12}$$

Evaluating the product of all D times, where $D >> 1$,

$$P = \prod_{s=1}^{S} \left[\frac{\sqrt{\pi}}{(1-g_s^2)^{\frac{n_s}{2}}} \frac{(1-g_s^2)^{\frac{1}{2}}}{(n_s g_s^2 + (1-g_s^2))^{\frac{1}{2}}}\right]^D \tag{B13}$$
$$\times \exp\left[\frac{g_s^2}{2(n_s g_s^2 + (1-g_s^2))(1-g_s^2)} \left(\sum_{d}^{D}\sum_{i\in s}^{n_s} X_i\right)^2\right] \tag{B14}$$
$$\times \exp\left[-\frac{1}{2}\frac{1}{1-g_s^2}\sum_{d}^{D}\sum_{i\in s}^{n_s} X_i^2\right]. \tag{B15}$$

Using that $C_{ij} = \frac{1}{D}\sum_d X_i X_j$,

$$\sum_{d}^{D}\left(\sum_{i\in s} X_i\right)^2 = \sum_{i,j=1}^{N}\left(\sum_{d}^{D} X_i X_j\right)\delta_{s_i s}\delta_{s_j,s} = Dc_s, \tag{B16}$$

and that the variance of the process in the sth cluster can be computed from the trace†

$$\sum_{i\in s}\sum_{d}^{D} X_i^2 = DC_{ii} = \sum_{i\in s}^{n_s} DC_{ii} = Dn_s. \tag{B18}$$

Substituting equations (B16) and (B18) into equation (B15),

$$P = \prod_{s=1}^{S} \left[\frac{\sqrt{\pi}}{(1-g_s^2)^{\frac{n_s}{2}}} \frac{(1-g_s^2)^{\frac{1}{2}}}{(n_s g_s^2 + (1-g_s^2))^{\frac{1}{2}}}\right]^D \times \exp\left[-\frac{D}{2}\frac{n_s}{1-g_s^2} + \frac{D}{2}\frac{c_s}{1-g_s^2}\frac{g_s^2}{n_s g_s^2 + (1-g_s^2)}\right] \tag{B19}$$

We can rewrite this as

$$P = \prod_{s=1}^{S} \frac{\pi^{\frac{D}{2}} (n_s g_s^2 + (1-g_s^2))^{\frac{-D}{2}}}{(1-g_s^2)^{\frac{D}{2}(n_s-1)}} \exp\left[-\frac{D}{2}\frac{1}{1-g_s^2}\left(n_s - \frac{c_s g_s^2}{n_s g_s^2 + (1-g_s^2)}\right)\right]. \tag{B20}$$

Then using that $P \propto e^{-DH_c}$, we can find $H_c \propto \ln(P)$ from equation (B20), and using that $\ln\prod_i A_i = \sum_i \ln(A_i)$ to find the log-likelihood

†The trace of the correlation matrix for each cluster s can be verified from the eigenvalues

$$\sum_{i}^{N} C_{ii} = \sum_{s}\lambda_s = (n_s-1)(1-g_s^2) + n_s g_s^2 + (1-g_s^2) = n_s. \tag{B17}$$

function [Need to use $D >> 1$ and look at expansion $(g_s - g_s^*)$]

$$\ln(P) = -\frac{D}{2}\sum_{s=1}^{S}\Big[\ln(n_s g_s^2 + (1-g_s^2)) \tag{B21}$$

$$+ (n_s - 1)\ln(1-g_s^2)\Big] \tag{B22}$$

$$+\frac{D}{2}\sum_{s=1}^{S}[\ln(\pi)] \tag{B23}$$

$$-\frac{D}{2}\sum_{s=1}^{S}\frac{1}{1-g_s^2}\left[n_s - \frac{c_s g_s^2}{n_s g_s^2 + (1-g_s^2)}\right]. \tag{B24}$$

Using equation (A11), we can substitute for g_s in (A11) to find the log-likelihood entirely in terms of n_s and c_s, using that $(1-g_s^2) = \frac{n_s^2 - c_s}{n_s^2 - n_s}$ and $\frac{c_s}{n_s} = n_s g_s^2 + (1-g_s^2)$:

$$H_c = \frac{1}{2}\sum_{s:n_s>0}\left[\log\frac{c_s}{n_s} + (n_s-1)\log\frac{n_s^2 - c_s}{n_s^2 - n_s}\right] + \frac{1}{2}\sum_{s:n_s>0}[\ln(\pi) + n_s]\,. \tag{B25}$$

The last term is a constant, given that $\sum_{s:n_s>0} n_s = N$ where N is the number of objects. This is fixed for a given system. Hence the likelihood function required is

$$H_c = \frac{1}{2}\sum_{s:n_s>0}\left[\log\frac{c_s}{n_s} + (n_s-1)\log\frac{n_s^2 - c_s}{n_s^2 - n_s}\right] \tag{B26}$$

up to a constant $\frac{1}{2}(S\ln(\pi) + N)$.